Unclassified

SECTION COPY

NACA

RESEARCH MEMORANDUM

STUDIES OF THE FLOW FIELD BEHIND A LARGE SCALE

47.5° SWEPTBACK WING HAVING CIRCULAR-ARC

AIRFOIL SECTIONS AND EQUIPPED WITH

DROOPED-NOSE AND PLAIN FLAPS

By Roy H. Lange and Marvin P. Fink

Langley Aeronautical Laboratory
Langley Field, Va.

NATIONAL ADVISORY COMMITTEE
FOR AERONAUTICS

WASHINGTON

March 10, 1952

NATIONAL ADVISORY COMMITTEE FOR AERONAUTICS

RESEARCH MEMORANDUM

STUDIES OF THE FLOW FIELD BEHIND A LARGE SCALE

47.5° SWEPTBACK WING HAVING CIRCULAR-ARC

AIRFOIL SECTIONS AND EQUIPPED WITH

DROOPED-NOSE AND PLAIN FLAPS

By Roy H. Lange and Marvin P. Fink

SUMMARY

An investigation of the effects of separation vortex flow on the downwash, sidewash, and wake characteristics behind a 47.5° sweptback wing having symmetrical circular-arc airfoil sections has been conducted in the Langley full-scale tunnel at a Reynolds number of 4.3×10^6 and a Mach number of 0.07. Three configurations were investigated through a large angle-of-attack range: namely, the basic wing, the wing with full-span drooped-nose flaps deflected 40°, and the wing with semispan plain flaps and full-span drooped-nose flaps deflected 40°. Charts showing vectors of downwash and sidewash angle and contours of dynamic-pressure ratio are presented for three longitudinal distances behind the wing which cover the range of possible locations of the empennage. The spanwise distribution of vorticity along the trailing vortex sheet has been determined from line integrations of the downwash and sidewash data. Integrations of the data have also been made to determine the variations with angle of attack of average downwash angle and dynamic-pressure ratio for a horizontal tail assumed to be located at several heights above and below the chord plane. Calculations of the downwash behind the wing in the plane of symmetry and at 0.28 semispans from the plane of symmetry, based on lifting line methods and utilizing experimentally determined span load distributions, are compared with the experimental downwash.

The results show that the separation vortex has a large effect on the flow inclination, wake, and spanwise distribution of vorticity behind the basic wing configuration. The delay in the formation of the separation vortex to high angles of attack caused by drooped-nose flap-deflection results in a smoothly varying distribution of downwash and vorticity across the wing semispan.

The variations with angle of attack of average downwash angle and average dynamic-pressure ratio indicate that the most desirable horizontal-tail location would be below the chord plane extended for all configurations investigated.

The correlation between the measured and calculated downwash indicates that the actual rather than the theoretical span load distribution should be used to calculate the downwash behind wings of this type.

INTRODUCTION

The phenomenon of separation vortex flow has been observed at low speeds on sweptback wings at high angles of attack and has been shown to greatly influence the aerodynamic characteristics of these wings. The sweptback wing considered in this paper presents a special case of the separation vortex flow because of the sharp leading-edge airfoil sections of the wing. Figure 1 shows the vortex represented schematically by a ribbon on one wing semispan and the corresponding pressure distribution on the other wing semispan (reference 1). Because of the sharp leading edge, the separation vortex existed at very low angles of attack, and the opportunity was taken to measure the flow field behind the wing and thus determine the influence of the separation vortex on the downwash and wake characteristics throughout the angle-of-attack range. Moreover, since the span load distribution had been measured previously (reference 1), this actual span loading was used in the calculation of the downwash for comparison with the measured downwash. Although the flow separation for the subject wing with the sharp leading edge represents an extreme case, it is useful in illustrating the effects of the separation-vortex type of flow. The flow characteristics of the subject wing are believed to represent qualitatively those to be obtained for highly sweptback wings having thin conventional airfoil sections with correspondingly small leading-edge radii.

The investigation included measurements at a Reynolds number of 4.3×10^6 and a Mach number of 0.07 of the downwash angle, sidewash angle, and dynamic pressure in a vertical plane at three longitudinal distances behind the wing which cover the range of possible locations of an empennage. The configurations tested through large angle-of-attack range include the basic wing (flaps neutral), the wing with full-span drooped-nose flaps deflected 40°, and the wing with full-span drooped-nose flaps and inboard semispan plain flaps deflected 40°.

COEFFICIENTS AND SYMBOLS

C_L lift coefficient (Lift/qS)

C_m pitching-moment coefficient $(\text{Pitching moment}/qS\bar{c})$

$\dfrac{c_l c}{C_L c_{av}}$ span loading coefficient

P pressure coefficient $\left(\dfrac{p - p_o}{q}\right)$

c_l section lift coefficient

α angle of attack of wing root chord, degrees

q free-stream dynamic pressure, pounds per square foot $\left(\dfrac{\rho}{2}V^2\right)$

S wing area, square feet

c local chord, feet

c_{av} average chord, feet (S/b)

b wing span, feet

p local static pressure, pounds per square foot

p_o free-stream static pressure, pounds per square foot

V free-stream velocity, feet per second

ρ mass density of air, slugs per cubic foot

q_t local stream dynamic pressure, pounds per square foot

y lateral distance from plane of symmetry, feet

c' chord perpendicular to line of maximum thickness, feet

$\bar{c}$ mean aerodynamic chord measured parallel to plane of symmetry

$$(8.37 \text{ ft})\ \left(\frac{2}{S}\int_0^{b/2} c^2 dy\right)$$

ϵ　　　　　　　local downwash angle, degrees

σ　　　　　　　local sidewash angle, inflow positive, degrees

q_t/q　　　　　ratio of local stream dynamic pressure to free-stream dynamic pressure

Γ　　　　　　　vorticity, square feet per second

Integrated air-stream surveys:

$(q_t/q)_{av}$　　average q_t/q, obtained by

$$\left[(q_t/q)_{av} = \frac{2}{S_t} \int_0^{b_t/2} (q_t/q) \ c_t \ dy_t \right]$$

ϵ_{av}　　　　average ϵ, obtained by

$$\left[\epsilon_{av} = \frac{2}{(q_t/q)_{av} S_t} \int_0^{b_t/2} \epsilon(q_t/q) \ c_t \ dy_t \right]$$

where

c_t　　　　　chord of tail, feet

b_t　　　　　span of tail, feet

S_t　　　　　area of tail, square feet

y_t　　　　　spanwise distance, feet

$d\epsilon_{av}/d\alpha$　　rate of change of ϵ_{av} with angle of attack, per degree

MODEL AND APPARATUS

Model

The geometric characteristics of the wing are given in figure 2. The wing has an angle of sweepback of 45° at the quarter-chord line or 47.5° sweep at the leading edge, an aspect ratio of 3.5, a taper ratio of 0.5, and has no geometric dihedral or twist. The airfoil section of the wing is a symmetrical, 10-percent-thick, circular-arc section

perpendicular to the 50-percent chord line. The wing was constructed of $\frac{1}{4}$ - inch aluminum sheet reinforced by steel channel spars. The wing construction is extremely rigid and it is believed that no deflections of an appreciable magnitude occurred during the tests.

The wing is equipped with full-span drooped-nose flaps and inboard semispan plain flaps which are 20 percent of the chord measured perpendicular to the line of maximum thickness. These flaps are pivoted on piano hinges mounted flush with the lower wing surface and, when deflected, produce a gap on the upper wing surface which is covered and faired with a sheetmetal seal. The drooped-nose and semispan plain flaps are deflected 40° measured normal to the hinge line.

Apparatus

The experimental arrangement is illustrated in figure 3 which shows the wing mounted in the Langley full-scale tunnel with the survey apparatus behind it. A photograph of the five-tube survey rake is shown in figure 4, and details of the combined pitch, yaw, and dynamic pressure tube are given in figure 5. The five-tube survey rake had been previously calibrated through a wide range of pitch and yaw angles. The survey apparatus maintained the five-tube rake vertical as it was moved laterally. In the low and moderate pitch and yaw angle range the downwash and sidewash angles are accurate to within about ±0.25°, and the dynamic pressure measurements are accurate to within about ±1 percent. The accuracy of measurement is decreased somewhat in the high angle ranges.

TESTS AND CORRECTIONS

Tests

The tests were made through an angle-of-attack range from about 3° to 26° at a Reynolds number of about 4.3×10^6 based on the mean aerodynamic chord and at a Mach number of 0.07. At each angle of attack the pressures acting on the combined pitch, yaw, and dynamic pressure tubes were measured on a multiple-tube manometer and photographically recorded. These measurements were made in a vertical plane at three longitudinal distances behind the wing ($0.925\bar{c}$, $1.425\bar{c}$, and $1.925\bar{c}$ from $\bar{c}/4$). In each vertical plane the survey points were spaced 1 foot in the spanwise direction and 6 inches in the vertical direction. Figure 6 shows the longitudinal location of the vertical survey planes as well as the spanwise extent of the surveys. The extent of the surveys

in the vertical direction was from 6 feet above to $4\frac{1}{2}$ feet below the chord plane extended. Inasmuch as all tests were made at $0°$ yaw, the surveys were made behind the left wing semispan only.

Corrections

All the data have been corrected for the blocking effects and for the air-stream misalinement. Surveys of the downwash in the jet with the wing removed were made at the $0.925\bar{c}$ and $1.925\bar{c}$ survey planes and were located vertically on the tunnel center line and for a lateral range which covered the wing semispan. From these surveys an average value of downwash angle was obtained at each survey plane and was applied as a constant throughout the vertical range of the surveys. There is some question as to the validity of applying such corrections to the data since it is not known how accurately these corrections apply to the entire flow field covered by the surveys. No corrections have been applied to the lift data for the tares and interference due to the wing supports, inasmuch as tare tests showed these effects to be negligible. The angles of attack have also been corrected for jet-boundary effects. The air-stream survey data have been corrected for jet-boundary effects which consist of an angle change to the downwash as given below:

Longitudinal survey location	$\Delta\epsilon$ (deg)
$0.925\bar{c}$	$-2.06C_L$
$1.425\bar{c}$	$-2.43C_L$
$1.925\bar{c}$	$-2.59C_L$

The jet-boundary corrections were determined by the methods given in reference 2. A study of the experimental downwash-correction data presented in reference 3 indicates that this theoretical jet-boundary correction would be adequate for the range of the present surveys.

PRESENTATION OF DATA

The downwash and wake results (figs. 7 to 39) are outlined in table I in order to facilitate the discussion.

RESULTS AND DISCUSSION

Air-Stream Surveys

The air-stream survey data are given in the form of vectors of resultant flow angularity and contours of dynamic-pressure ratio. The vertical component of the vector is the downwash angle in degrees, and the horizontal component is the sidewash angle in degrees.

The effect of the wing support struts on the flow at the survey planes is indicated on the lower part of each figure by the areas of reduced dynamic-pressure ratio in the region between 6 feet and 8 feet from the plane of symmetry. These wakes are not considered, however, to otherwise appreciably affect the flow field. The discussion of the air-stream surveys will be concerned primarily with the results obtained at the rearmost survey plane (1.925$\bar{c}$), and the data at the two other survey planes are included to indicate the typical progression of the flow downstream from the wing trailing edge.

Basic wing.- The air-stream surveys for an angle of attack of 2.9° (fig. 12) show a well-defined wake region, and the tip vortex is weak but clearly evidenced by the clockwise rotation of the vectors in the tip region. The line of intersection of the trailing vortex sheet with the plane of survey (where there is an abrupt change from a general inflow to a general outflow) coincides roughly with the wake or measured region of least dynamic-pressure ratio. At this low angle of attack the previous flow studies and pressure-distribution measurements of the wing (reference 1 and fig. 8) show evidence of flow separation at the outermost spanwise station (0.80b/2).

Increasing the angle of attack to 6.6° (fig. 13) results in larger values of downwash angle (in general about 7° in the region above the chord plane extended), and the tip vortex is seen to be stronger than for the previous angle of attack. The flow studies and pressure distributions (fig. 8) at this angle of attack show that the separation vortex has formed along the wing leading edge but that the chordwise extent of flow separation is much greater at the tip. Inspection of the contours of dynamic-pressure ratio shows a narrow region of reduced dynamic pressure which extends about 2 feet inboard of the wing tip and which, presumably, reflects the influence of the tip separation. As was noted for the previous angle of attack, the trailing vortex sheet is located roughly in the wake region indicated by the contours of dynamic-pressure ratio.

At an angle of attack of 10.2°, the results of reference 1 show that the 0.80b/2 station has attained maximum lift, but the rather flat chordwise pressure distribution measured at that station (fig. 8)

indicates that the separation vortex has been shed off the wing trailing
edge somewhat inboard of this point. Outboard of 0.80b/2 the flow
studies indicated complete stall. The influence of the separation vortex
is clearly evidenced in the air-stream surveys by the somewhat confused
distribution of both wake and vorticity in the region near the wing tip.
(See fig. 14.) The large unsymmetrical region of reduced dynamic-
pressure ratio which extends about 4 feet inboard of the wing tip indi-
cates that the separation and tip vortices have merged into one large
distorted vortex. The downwash angles on the inboard side of the sepa-
ration vortex attain values of 20°, whereas on the outboard side the
sidewash angles are about 12°. The location of the trailing vortex
sheet is not clearly defined but appears to be located about 2.25 feet
above the chord plane extended. The contours of dynamic-pressure ratio
are in good agreement with this location for the wake only for the region
near the plane of symmetry.

The line of intersection of the trailing vortex sheet with the
plane of survey is not clearly defined from the vector fields of down-
wash and sidewash. This difficulty results from the spanwise flow of
the boundary-layer air toward the tips peculiar to sweptback wings.
This outflow is particularly strong on the upper-wing surface. Accord-
ingly, the main discontinuity in spanwise component occurs near the top
of the wake (where the vectors above the wake point inward and those at
the top of the wake point outward) instead of near the center of the
wake as for unswept wings. The apparent location of the trailing vortex
sheet, therefore, does not always agree with the location of the wake
center line as determined from the dynamic-pressure measurements. This
effect is shown more clearly in the surveys made close to the wing
trailing edge. (See figs. 15 and 16.)

Increasing the angle of attack to 14° causes the core of the sepa-
ration vortex to be swept farther inboard to about 9.5 feet (or 0.64b/2)
from the plane of symmetry (fig. 17). The corresponding span load dis-
tribution of the wing (fig. 9) shows an increase in loading at the
40-percent station and a large decrease in loading outboard of the
70-percent station associated with the stall of the wing outboard of
this point. As further shown in the upper half of figure 17 there is a
region of negative vorticity indicated at about 12.5 feet from the plane
of symmetry and about 3 feet above the chord plane extended. As shown
by the contours of dynamic-pressure ratio, the tip vortex and the sepa-
ration vortex each maintains its identity, and there is a region of rel-
atively high dynamic-pressure ratio between the two trailing vortices.
Although stalled, the tip region is still contributing to the lift of the
wing. It is interesting to note at this relatively high angle of attack
that the measured wake is very weak for the inboard 50 percent of the
span. The location of the inboard portion of the trailing vortex sheet
is not clearly defined but appears to be located about 2.75 feet above the
chord plane extended, and, therefore, its location is on about the same

level as the center of rotation of the two trailing vortices. Apparently the characteristic curved or channel-shaped cross section of the trailing vortex sheet far behind unswept wings, with the tip vortices well above the middle region, does not exist behind the present sweptback wing. The reason may be that the tip vortices of sweptback wings leave the wing initially at a level considerably below that of the wake from the root sections.

At the highest angle of attack investigated $\alpha = 18^\circ$ (fig. 18) the core of the separation vortex has moved inboard to about $0.60b/2$, and in this region the span load distributions show the greatest decrease in loading as compared with that obtained at $\alpha = 14^\circ$. The separation vortex and tip vortex have increased in intensity, and downwash angles of over 35° and sidewash angles of over 20° are measured around the separation vortex. The negative vorticity between the two trailing vortices is again indicated but the flow field is more confused than that obtained at $\alpha = 14^\circ$. More than half of the outboard semispan is affected by the reduced dynamic-pressure ratio region of the two vortices, but the wake is weak over the inboard 40 percent of the semispan. The location of the trailing vortex sheet is very difficult to determine, and again the surveys made closer to the wing (figs. 19 and 20) show the effects of the spanwise flow of the boundary layer on the wake shed from the wing trailing edge. At this angle of attack the lift coefficient is 0.80 which is 92 percent of the maximum lift coefficient; however, the pitching-moment data (fig. 7) indicate an aerodynamic center shift of about $0.15\overline{c}$ as compared with the lower angles of attack. There is therefore a question as to whether this is a flyable attitude.

Effect of drooped-nose flap deflection.- The marked improvement in the flow over the wing due to the delay in the formation of the separation vortex caused by drooped-nose flap deflection, shown in reference 1, is reflected in the air flow measurements behind the wing. (Compare figs. 21 to 25 with figs. 13 to 18.) At the lower angles of attack the downwash distribution at a given height varies gradually across the wing semispan except, of course, near the wing tip. The downwash field obtained is a result of a more uniform distribution of loading over the wing as compared with that obtained for the basic wing. As shown in figure 10, the load distribution approaches the calculated theoretical additional loading based on the potential-flow method of reference 4. The tip vortex is weak but clearly evident for angles of attack of 14.4° and 18.2° (figs. 21 and 23), and the loss in dynamic-pressure in the wake is small. The wake center line at the midsemispan stations is located above the chord plane extended at about 1.50 feet for $\alpha = 14.4^\circ$, 2.25 feet for $\alpha = 18.2^\circ$, and 4.00 feet for $\alpha = 22.0^\circ$. The pressure distribution measurements (reference 1) indicated the presence of the separation vortex at 11.4 feet from the plane of symmetry $(0.80b/2)$ at $\alpha = 22.0^\circ$, and this result is indicated by the region of reduced dynamic-pressure ratio near the tip in figure 24. The previous pressure

distribution measurements further showed that the separation vortex
covered the entire wing outboard of the 20-percent station at $\alpha = 25.8°$.
The data from the present investigation at $\alpha = 25.8°$ (not shown)
showed that the influence of the separation vortex extended from about
50 percent of the semispan outboard to the tip and induced downwash and
sidewash angles beyond the calibration of the survey rake. (ϵ, $\sigma > 40°$)

Effect of combined drooped-nose and plain flap deflection.- Deflec-
tion of the semispan plain flaps in combination with the drooped-nose
flaps produces wake patterns quite different from those obtained with
the drooped-nose flaps deflected alone. (See figs. 26 to 28.) At an
angle of attack of $8.3°$ the low total-pressure region behind the semi-
span plain flap is clearly evident and is confined to the inboard semi-
span region; however, with increase in angle of attack to $15.9°$ (fig. 27)
the wake from the plain flaps is shifted outboard and lies between
$0.35b/2$ and $0.70b/2$ from the plane of symmetry. The downwash and side-
wash fields for these two angles of attack show the effect of the
drooped-nose flaps in preventing the formation of the separation vortex,
but there is an increase in downwash in the inboard spanwise stations
as compared with the outboard stations associated with the influence of
the semispan plain flaps. At the highest angle of attack investigated
($\alpha = 21.5°$), however, the separation vortex has trailed off the wing at
about 10 feet from the plane of symmetry (or about $0.70b/2$), and the flow
field is similar to that obtained for the basic wing at high angles of
attack. As shown in figures 26 to 28 there is no evidence of a concen-
trated vortex being shed from the tip of the plain flap, a result which
may have been expected on the basis of past experience with unswept wings.
The results of figures 26 to 28 are, however, in agreement with the
smoothly varying spanwise load distributions near the flap-tip region.
(See fig. 11.)

Distribution of Vorticity

As discussed in reference 5 it is possible to determine the span-
wise distribution of vorticity along the trailing vortex sheet by
integrating the tangential component of the velocity along the boundary
of a closed area of the plane of survey. The quantities integrated are
$V_L \sin \epsilon\ dr$ along the vertical sides and $V_L \sin \sigma\ dr$ along the hori-
zontal sides, where ϵ and σ are the experimentally determined down-
wash and sidewash angles, V_L is the local airspeed, and dr is the
length of the side. Such integrations have been made for pertinent angles
of attack for the three configurations investigated, and the results
are given in figures 29 and 30. In general, the integrations were made
around one-foot-square blocks.

As shown in figure 29, the region of maximum vorticity moves rapidly inboard from the wing tip with increasing angle of attack for the basic wing configuration. Calculations show that the amount of vorticity shed in the tip-vortex region is only a fraction of that shed in the separation-vortex region at the high angles of attack. At $\alpha = 14.0^\circ$ where the trailing separation vortex and tip vortex each maintains its identity, the region of maximum vorticity lies between 9 and 10 feet from the plane of symmetry and there is a clockwise rotation of the flow field. Between 12 and 13 feet from the plane of symmetry, however, there is a counterclockwise rotation of the flow field associated with the negative vorticity shed between the trailing separation vortex and tip vortex. This negative vorticity is equal in magnitude to the vorticity shed in the tip vortex region.

As expected, deflection of the drooped-nose-flap results in a more normal distribution of vorticity such that the region of maximum vorticity (and hence rolling up) occurs near the wing tip. (See fig. 30(a).) The region of maximum vorticity also occurs near the wing tip with the semispan plain flaps deflected in combination with the drooped-nose flaps for angles of attack up to 15.9°. (See fig. 30(b).) For angles of attack greater than 15.9°, however, the air-stream survey charts indicate that the distribution of vorticity would be similar to that obtained for the basic wing at high angles of attack.

Average Values of Downwash and Dynamic-Pressure Ratio

In order to provide data of a quantitative nature which may be useful for design purposes, the air-stream survey data (downwash angles and dynamic-pressure ratios) have been weighted according to the chord and averaged by integration across the span of a horizontal tail, assumed to be located $2.06\overline{c}$ behind the wing, as shown in figure 31. The horizontal tail is similar to the wing in plan form, but its linear dimensions are three-eighths of those of the wing. Average values of downwash angle and dynamic-pressure ratio were determined for several tail heights varying from 3 feet above the chord plane extended to 2 feet below the chord plane extended.

In the range of high angles of attack, which is of primary interest for this low-speed investigation, the results presented in figure 32 show that the most desirable location for the horizontal tail is below the chord plane extended, for in this position the lowest values of $d\epsilon_{av}/d\alpha$ are obtained for the three configurations investigated. This result is in agreement with similar studies at large scale on wings of 42° and 52° sweepback (references 6 to 9). The 42° wing and the 52° wing with conventional sections did not have the separation vortex-type flow except for that noted at the tips of the 52° wing at high

angles of attack. The low tail position, therefore, appears to be most
desirable for wings with either type of flow. Stabilizing effects are
also indicated for locations above the chord plane extended for the
basic wing, for the high tail location with drooped-nose flaps deflected,
and on the chord plane for the drooped-nose and semispan plain flaps
configuration; however, the downwash angles are considerably lower for
the location below the chord plane extended.

The variations of average dynamic-pressure ratio with angle of
attack show only slight differences among the tail locations investi-
gated for the basic wing and drooped-nose flaps configurations. (See
figs. 32(a) and 32(b).) For the wing with drooped-nose flaps and semi-
span plain flaps deflected, there is a large reduction in $(q_t/q)_{av}$
at the low angles of attack (below 10°) for the tail locations above the
chord plane extended resulting from the wake from the semispan plain
flaps. (See fig. 32(c).) For angles of attack above 12° the lowest
values of $(q_t/q)_{av}$ were obtained with the tail located on the chord
plane extended.

Correlation with Theory

General methods for predicting the downwash and wake characteris-
tics behind unswept wings with flaps both neutral and deflected are
given in references 5 and 10, where it is shown that, in order to
realize satisfactory agreement between experiment and theory, the dis-
placement of the wake must be taken into account, but that the rolling-
up of the edges of the wake may be neglected. The aspect ratios of
sweptback wings, however, are lower than those of the unswept wings
heretofore considered; therefore there may be more rolling-up effect.
On the other hand, the tips of sweptback wings at angles of attack are
much lower than the center portions of the wing, and this effect would
tend to make the vortex sheet flat and would tend to reduce the rate of
rolling-up. An extension of the above methods for application to swept-
back wings, when the assumption is made that the bound vortex is swept-
back along the quarter-chord line of the wing, is given in reference 6.
The results of reference 6 for a 42° sweptback wing show that the cal-
culated downwash underestimates the experimental downwash at the plane
of symmetry but gives reasonable estimates of the experimental downwash
outboard of the plane of symmetry. Calculations of the downwash behind
the subject wing, based on the methods of reference 6, have been made
by utilizing the experimentally determined span load distributions and
are presented in figures 33 to 38 along with the experimental data for
the three wing configurations investigated. Included for comparison in
figure 33 are the calculated downwash angles based on the theoretical
span load distribution of the basic wing as obtained from reference 4.
The locations of the wake center lines given in figures 33 to 38 (and

also figs. 29 and 30) were determined from the air-stream-survey data, although, as mentioned previously, the intersections of the trailing vortex sheet with the plane of survey are not clearly defined in some instances.

Downwash.- The results obtained at the plane of symmetry are presented in figures 33 to 35 for the three configurations. For the basic wing configuration in the low angle-of-attack range ($\alpha = 2.9^O$ and 6.6^O) the experimental values of downwash are higher above the wake center line and lower below the wake center line than the calculated values. (See fig. 33.) At an angle of attack of 10.2^O the experimental and calculated values of downwash are in good agreement only for a small distance at the upper edge of the survey region and the experimental values then diverge from the calculated values below the wake center line. The peak in the downwash distribution at the wake center line calculated from the experimental span loadings at angles of attack of 10.2^O and 14.0^O is caused by the abrupt increase in loading measured at $0.05b/2$ (see fig. 9). In an attempt to improve the correlation, therefore, calculations were made with the irregular load distribution of the inboard stations replaced by a smooth curve which was tangent to the original loading at $0.30b/2$ and which was horizontal at the plane of symmetry and located so that the areas under the modified and original loading curves were equal. The resulting downwash distribution at $\alpha = 10.2^O$ was almost identical with that calculated from the theoretical span loading. The correlation for $\alpha = 14.0^O$ was improved slightly for locations at and below the wake center line only. The agreement between the experimental downwash and that calculated by using the experimental span loading is improved with further increase in angle of attack such that, at an angle of attack of 18.0^O, the agreement is good for all points at and below the wake center line. The downwash calculated from the theoretical span loading, however, underestimates the experimental values by from 10 percent to 88 percent throughout the vertical range at high angles of attack because the actual span loading is more concentrated near the plane of symmetry.

For the wing with flaps deflected the downwash calculated from the experimental span loading considerably underestimates the experimental downwash. The discrepancy at the wake center line increases from about 3° at the lower angles of attack to 6° at the highest angles of attack. (See figs. 34 and 35.) This discrepancy is attributed in part to the lack of sufficient spanwise stations to determine accurately the spanwise loading over the wing obtained from reference 1, especially for the combined flaps configuration where the span load distributions are more or less arbitrarily faired in the regions of $\frac{2y}{b} = 0.50$ and 0.90.

Calculations of the downwash at $\frac{2y}{b} = 0.28$ have been made in an
attempt to alleviate the effects of the abrupt loading changes noted
near the plane of symmetry for the basic wing configuration (fig. 9)
and the results for the three wing configurations are given in fig-
ures 36 to 38. The results for the basic wing configuration (fig. 36)
show, in general, an improvement between the calculated and experimental
values of downwash for angles of attack up to 14.0° as compared with the
results obtained at the plane of symmetry. The improvement in the
agreement between calculated and experimental downwash outboard of the
plane of symmetry was also noted in reference 6 and is discussed in the
downwash calculation procedure given in reference 11. For the wing with
drooped-nose flaps deflected 40° (fig. 37) the correlation is improved
considerably throughout the vertical range of the surveys and also
throughout the angle-of-attack range as compared with the results
obtained at the plane of symmetry. Reasonable estimates of the experi-
mental downwash are obtained for all points at and below the wake center
line for angles of attack up to 22.0°. The results obtained for the
combined flaps configuration (fig. 38) show no significant improvement
over the results obtained at the plane of symmetry.

In order to obtain a span load distribution for the basic wing
representative of the low angle-of-attack range, the irregularities in
loading at the inboard stations were diminished by averaging the
loadings obtained at angles of attack of 1.1°, 2.9°, 4.8°, and 6.6°.
This average span load distribution (shown in fig. 39) was utilized in
calculating downwash for angles of attack of 2.9° and 6.6° by taking into
account the corresponding lift coefficients and the results are presented
in figure 36. As shown in figure 36 the downwash calculated from the
average experimental span load distribution resulted in a substantial
improvement in the correlation at the wake center line and produced a
downwash distribution which was in good agreement with the experimental
values throughout most of the vertical range investigated. Use of the
average loading for calculating the downwash at the plane of symmetry,
however, provided no improvement in the correlation (not shown). These
results indicate the care which must be exercised in evaluating available
experimental span load distributions on wings of this type and also indi-
cate the desirability of obtaining more information concerning the
loading and flow phenomena over highly sweptback wings.

In summary, the results of the correlation indicate that a knowledge
of the actual span load distribution is essential to the calculation of
the downwash behind wings of this type. In general, the correlation at
the plane of symmetry was good for the region below the wake center line
for the basic wing and for the wing with the combination of drooped-nose
and plain flaps deflected. For the location outboard of the plane of
symmetry the correlation was good below the wake center line for the
basic wing and for the wing with drooped-nose flaps deflected. The

results indicate that the uncertainties in the wind-tunnel corrections could account for the discrepancies in the correlation for some of the conditions investigated; however, for the locations on and above the wake center line, especially for the flaps-deflected configurations, there is no satisfactory explanation at present for the large discrepancies obtained.

Wake displacement.- The locations of the intersections of the trailing vortex sheet (or wake center lines) with the plane of survey have been calculated by the methods given in reference 5 and are found to be in reasonably agreement with the measured locations at the lower angles of attack for each of the three configurations investigated. The measured location of the wake center line (above the chord plane extended) is, however, considerably higher than the calculated location in the moderate to high angle-of-attack range.

SUMMARY OF RESULTS

The studies of the flow field at low speed behind a large-scale 47.5° sweptback wing having circular-arc airfoil sections and with drooped-nose and plain flaps neutral and deflected 40° gave the following results:

1. At low angles of attack the separation vortex produces an odd-shaped wake region behind the basic wing near the tip which increases in size and spreads inboard with increasing angle of attack such that at high angles of attack ($\alpha \geq 14^{\circ}$) the trailing-tip vortex and separation vortex become more distinctly separated. In the high angle-of-attack range the wake is weak over the inboard 40 percent of the wing semispan. The region of maximum vorticity moves rapidly inboard from the tip with increasing angle of attack and the trailing vortex sheet is essentially flat inboard of this region.

2. The delay in the formation of the separation vortex to high angles of attack ($\alpha > 22^{\circ}$) caused by drooped-nose flap deflection results in a smoothly varying distribution of downwash and vorticity across the semispan. A strong vortex occurs only at the wing tip. With semispan plain flaps deflected in combination with drooped-nose flaps, the distribution of downwash and vorticity behind the wing for angles of attack up to 15.9° is similar to that obtained behind the wing with drooped-nose flaps deflected alone, and there is no evidence of a vortex being shed from the tip of the plain flap. At the highest angle of attack, ($\alpha = 21.5^{\circ}$), the separation vortex is shed off the wing at about $0.70b/2$.

3. The variations with angle of attack of average downwash angle and average dynamic-pressure ratio indicate that the most desirable tail location would be below the chord plane extended for all configurations investigated.

4. The correlation between the measured and calculated downwash indicates that a knowledge of the actual span load distribution is essential to the calculation of the downwash behind wings of this type. In general, the correlation is good for the region below the wake center line for the basic wing; however, for the flaps deflected configurations there are large discrepancies in the region at and above the wake center line which cannot be explained. The correlation is better outboard of the plane of symmetry than at the plane of symmetry.

Langley Aeronautical Laboratory
        National Advisory Committee for Aeronautics
                Langley Field, Va.

<div align="center">REFERENCES</div>

1. Lange, Roy H., Whittle, Edward F., Jr., and Fink, Marvin P.: Investigation at Large Scale of the Pressure Distribution and Flow Phenomena over a Wing with the Leading Edge Swept Back 47.5° Having Circular-Arc Airfoil Sections and Equipped with Drooped-Nose and Plain Flaps. NACA RM L9G15, 1949.

2. Katzoff, S., and Hannah, Margery E.: Calculation of Tunnel-Induced Upwash Velocities for Swept and Yawed Wings. NACA TN 1748, 1948.

3. Silverstein, Abe, and Katzoff, S.: Experimental Investigation of Wind-Tunnel Interference on the Downwash behind an Airfoil. NACA Rep. 609, 1937.

4. DeYoung, John: Theoretical Additional Span Loading Characteristics of Wings with Arbitrary Sweep, Aspect Ratio, and Taper Ratio. NACA TN 1491, 1947.

5. Silverstein, Abe, Katzoff, S., and Bullivant, W. Kenneth: Downwash and Wake behind Plain and Flapped Airfoils. NACA Rep. 651, 1939.

6. Furlong, G. Chester, and Bollech, Thomas V: Downwash, Sidewash, and Wake Surveys behind a 42° Sweptback Wing at a Reynolds Number of 6.8×10^6 with and without a Simulated Ground. NACA RM L8G22, 1948.

7. Foster, Gerald V., and Griner, Roland F.: A Study of Several Factors Affecting the Stability Contributed by a Horizontal Tail at Various Vertical Positions on a Sweptback-Wing Airplane Model. NACA RM L9H19, 1949.

8. Griner, Roland F., and Foster, Gerald V.: Low-Speed Longitudinal and Wake Air-Flow Characteristics at a Reynolds Number of 6.0×10^6 of a 52° Sweptback Wing Equipped with Various Spans of Leading-Edge and Trailing-Edge Flaps, a Fuselage, and a Horizontal Tail at Various Vertical Positions. NACA RM L50K29, 1951.

9. Foster, Gerald V., and Griner, Roland F.: Low-Speed Longitudinal and Wake Air-Flow Characteristics at a Reynolds Number of 5.5×10^6 of a Circular-Arc 52° Sweptback Wing with a Fuselage and a Horizontal Tail at Various Vertical Positions. NACA RM L51C30, 1951.

10. Silverstein, Abe, and Katzoff, S.: Design Charts for Predicting Downwash Angles and Wake Characteristics behind Plain and Flapped Wings. NACA Rep. 648, 1939.

11. Diederich, Franklin W.: Charts and Tables for Use in Calculations of Downwash of Wings of Arbitrary Plan Form. NACA TN 2353, 1951.

TABLE I.- OUTLINE OF FIGURES

| Configuration	Description	α (deg)	Figure	Source
Basic wing; drooped-nose flaps deflected; and drooped-nose flaps and semispan plain flaps	α against C_L; C_m against C_L	0 to 25.8	7	-----------
Basic wing	P against x/c	2.9 to 18.0	8	Reference 1
Basic wing	Span load distributions	1.1 to 19.9	9	Reference 1
Drooped-nose flaps	Span load distributions	10.7 to 25.8	10	Reference 1
Drooped-nose and semispan plain flaps	Span load distributions	4.5 to 21.5	11	Reference 1
Basic wing	Air-stream surveys at $1.925\bar{c}$	2.9	12	-----------
Basic wing	Air-stream surveys at $1.925\bar{c}$	6.6	13	-----------
Basic wing	Air-stream surveys at $1.925\bar{c}$	10.2	14	-----------
Basic wing	Air-stream surveys at $0.925\bar{c}$	10.2	15	-----------
Basic wing	Air-stream surveys at $1.425\bar{c}$	10.2	16	-----------
Basic wing	Air-stream surveys at $1.925\bar{c}$	14.0	17	-----------
Basic wing	Air-stream surveys at $1.925\bar{c}$	18.0	18	-----------
Basic wing	Air-stream surveys at $0.925\bar{c}$	18.0	19	-----------
Basic wing	Air-stream surveys at $1.425\bar{c}$	18.0	20	-----------
Drooped-nose flaps	Air-stream surveys at $1.925\bar{c}$	14.4	21	-----------
Drooped-nose flaps	Air-stream surveys at $0.925\bar{c}$	14.4	22	-----------
Drooped-nose flaps	Air-stream surveys at $1.925\bar{c}$	18.2	23	-----------
Drooped-nose flaps	Air-stream surveys at $1.925\bar{c}$	22.0	24	-----------
Drooped-nose flaps	Air-stream surveys at $0.925\bar{c}$	22.0	25	-----------
Drooped-nose and semispan plain flaps	Air-stream surveys at $1.925\bar{c}$	8.3	26	-----------
Drooped-nose and semispan plain flaps	Air-stream surveys at $1.925\bar{c}$	15.9	27	-----------
Drooped-nose and semispan plain flaps	Air-stream surveys at $1.925\bar{c}$	21.5	28	-----------
Basic wing	Distribution of vorticity	6.6 to 14.0	29	-----------
Drooped-nose flaps and drooped-nose and semispan plain flaps	Distribution of vorticity	14.4 and 15.9	30	-----------
--------------------------	Location of assumed tail	--------------	31	-----------
Basic wing; drooped-nose flaps; drooped-nose and semispan plain flaps	ϵ_{av} and $\left(\dfrac{q_t}{q}\right)_{av}$	2.9 to 25.8	32	-----------
Basic wing	Experimental and calculated ϵ	2.9 to 18.0	33	-----------
Drooped-nose flaps	Experimental and calculated ϵ	14.4 to 25.8	34	-----------
Drooped-nose and semispan plain flaps	Experimental and calculated ϵ	8.3 to 21.5	35	-----------
Basic wing	Experimental and calculated ϵ, $2y/b = 0.28$	2.9 to 18.0	36	-----------
Drooped-nose flaps	Experimental and calculated ϵ, $2y/b = 0.28$	14.4 to 25.8	37	-----------
Drooped-nose and semispan plain flaps	Experimental and calculated ϵ, $2y/b = 0.28$	8.3 to 21.5	38	-----------
Basic wing	Average span load distribution	--------------	39	-----------
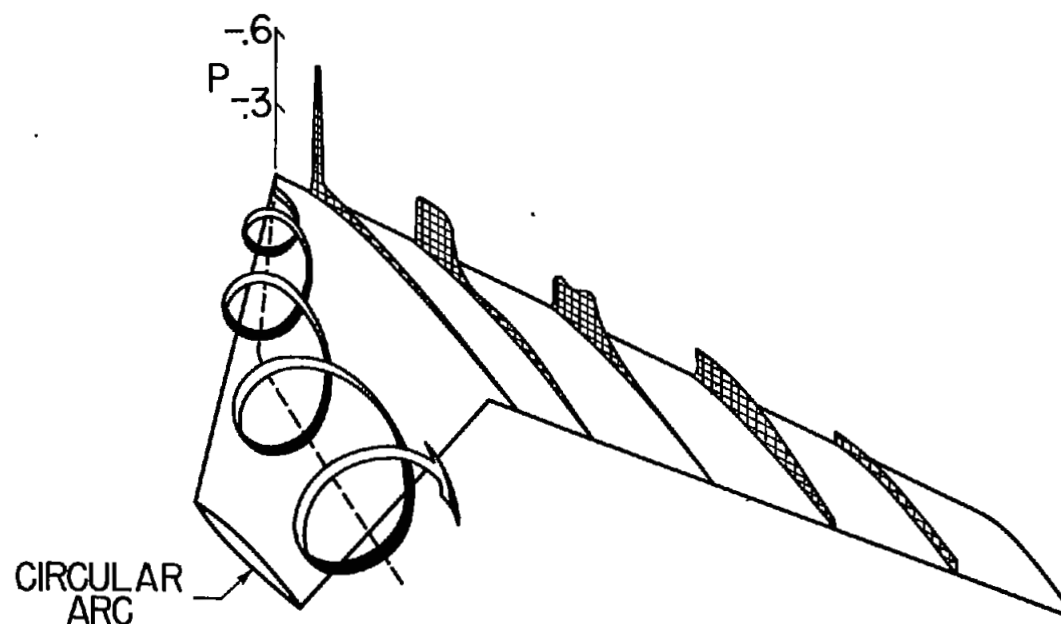
Figure 1.- Separation vortex represented schematically by ribbon and corresponding pressure distribution on 47.5° sweptback wing with flaps neutral. $\alpha = 12.1^\circ$; $C_L = 0.64$.
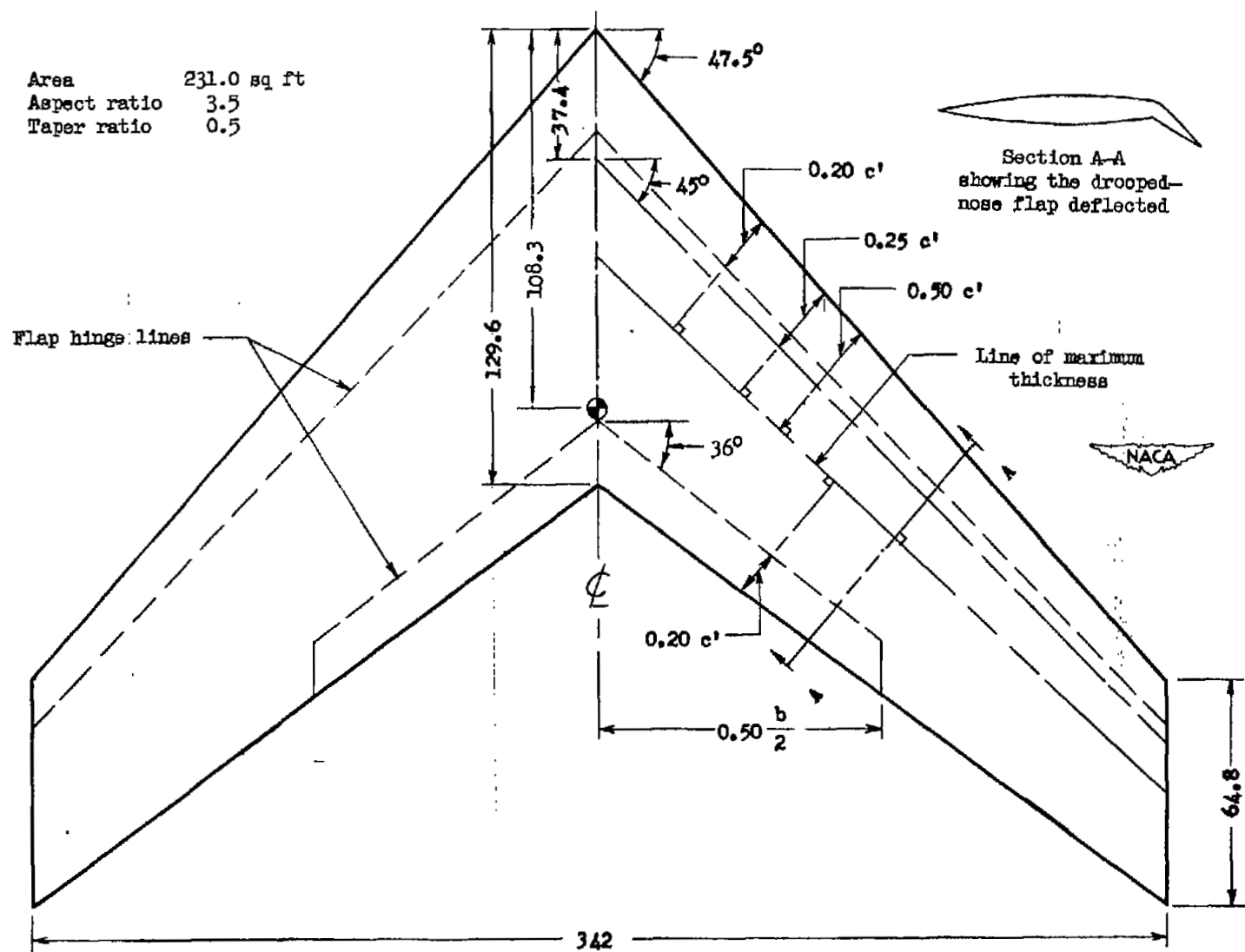
Area	231.0 sq ft
Aspect ratio	3.5
Taper ratio	0.5

47.5°

37.4

45°

108.3

129.6

0.20 c'

0.25 c'

0.50 c'

Section A-A
showing the drooped-
nose flap deflected

Flap hinge lines

Line of maximum
thickness

36°

0.20 c'

$0.50 \frac{b}{2}$

64.8

342

Figure 2.- Plan form of $47.5°$ sweptback wing. All dimensions are in inches.
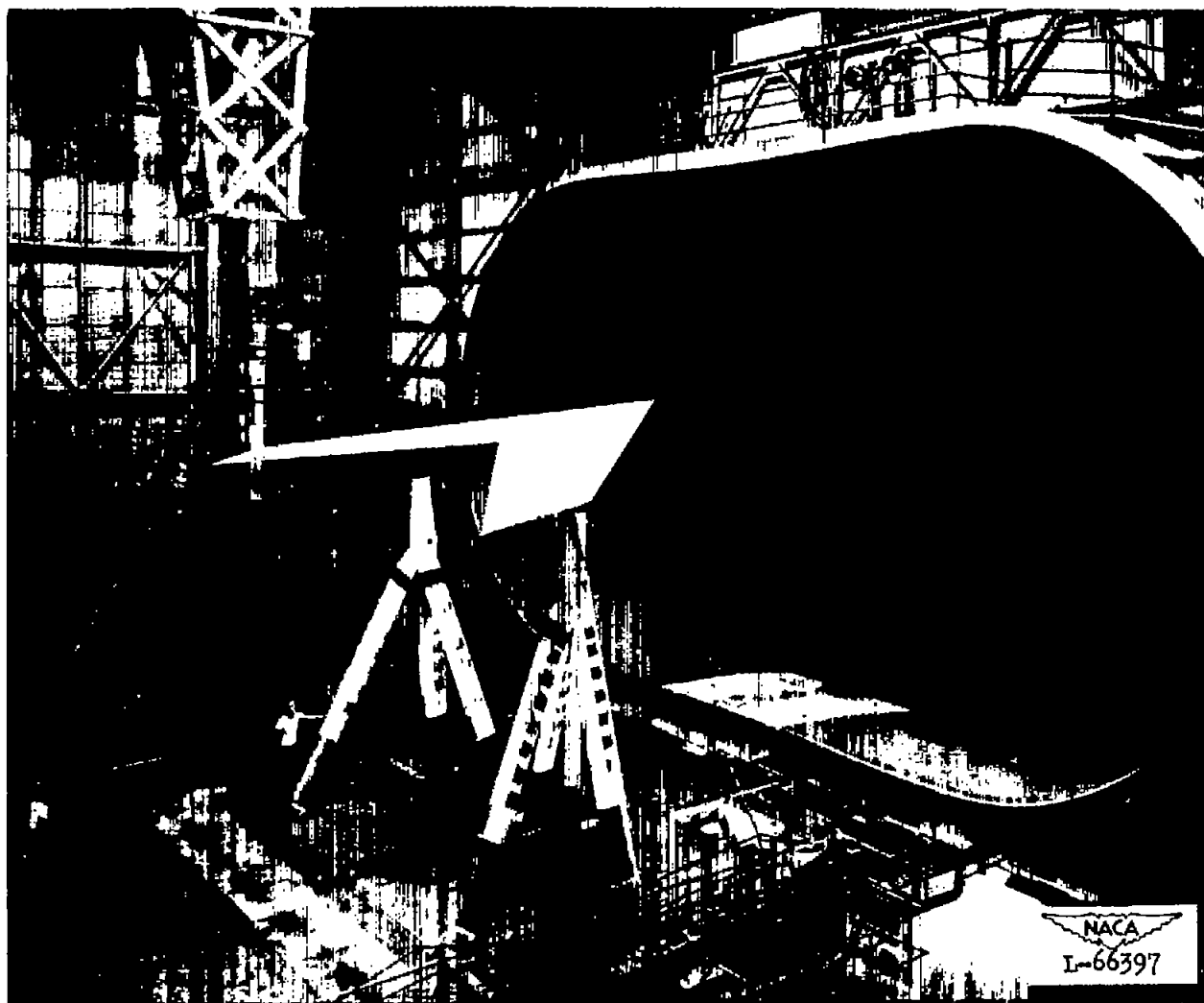
Figure 3.- The 47.5° sweptback wing mounted in the Langley full-scale
tunnel with survey apparatus behind wing.
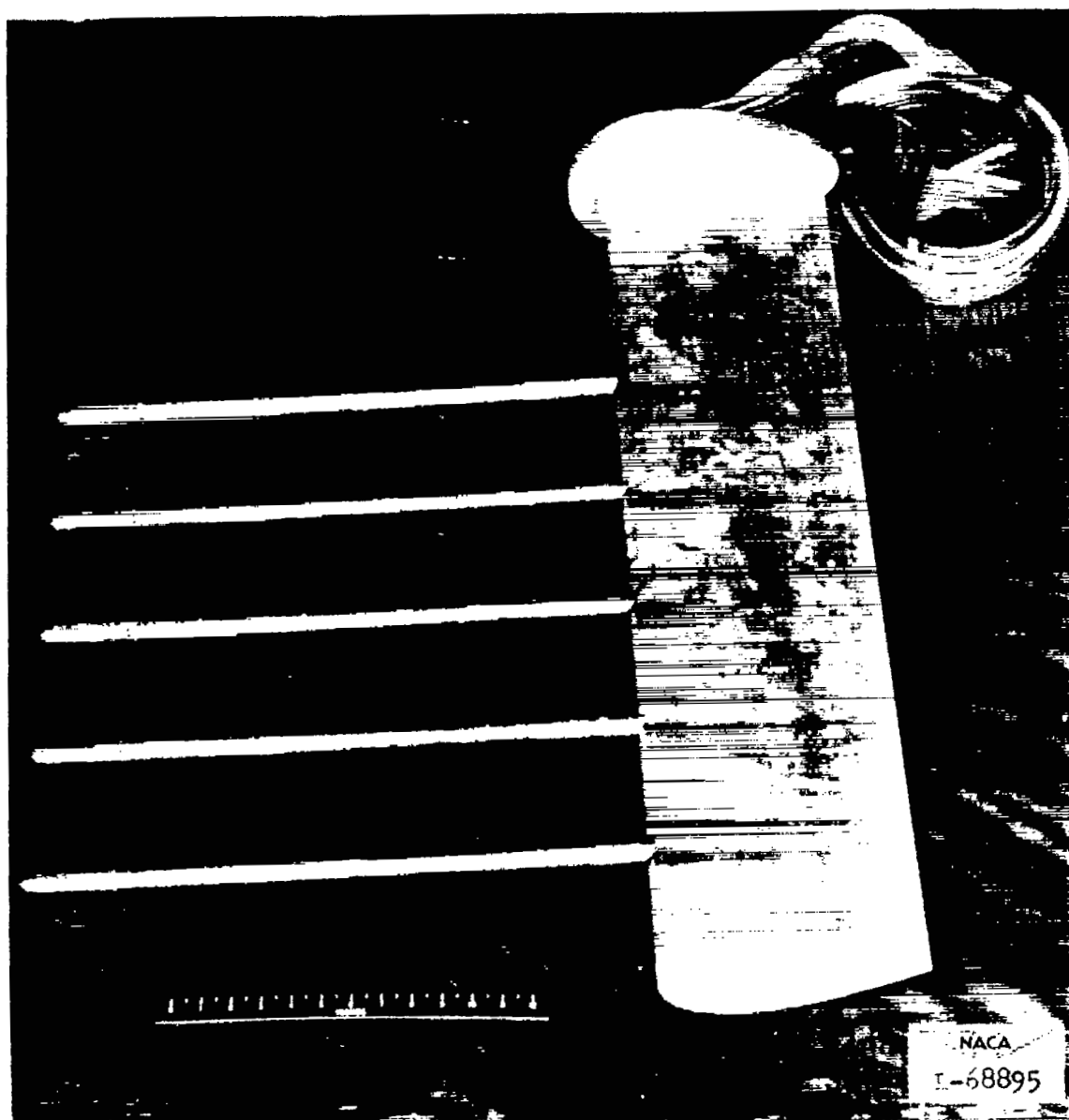
Figure 4.- The five-tube survey rake.
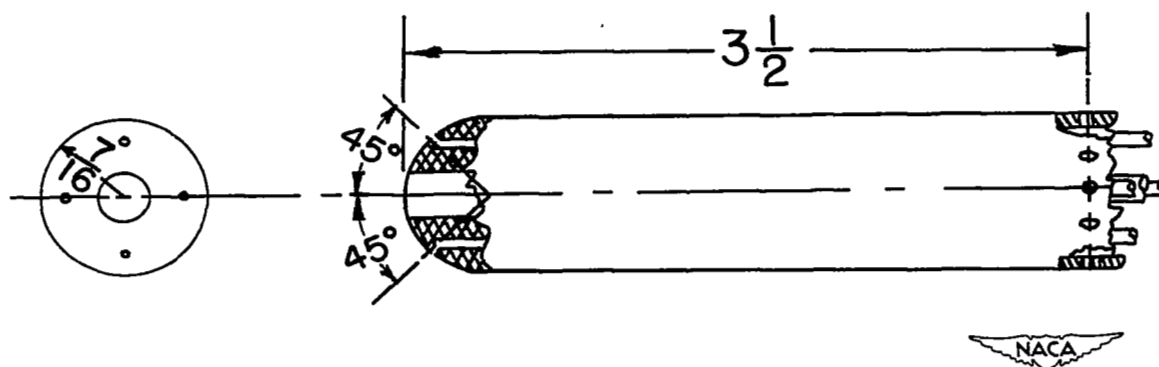
Figure 5.- Line drawing of combined pitch, yaw, and pitot-static tube
used for the air-stream surveys. All dimensions are in inches.
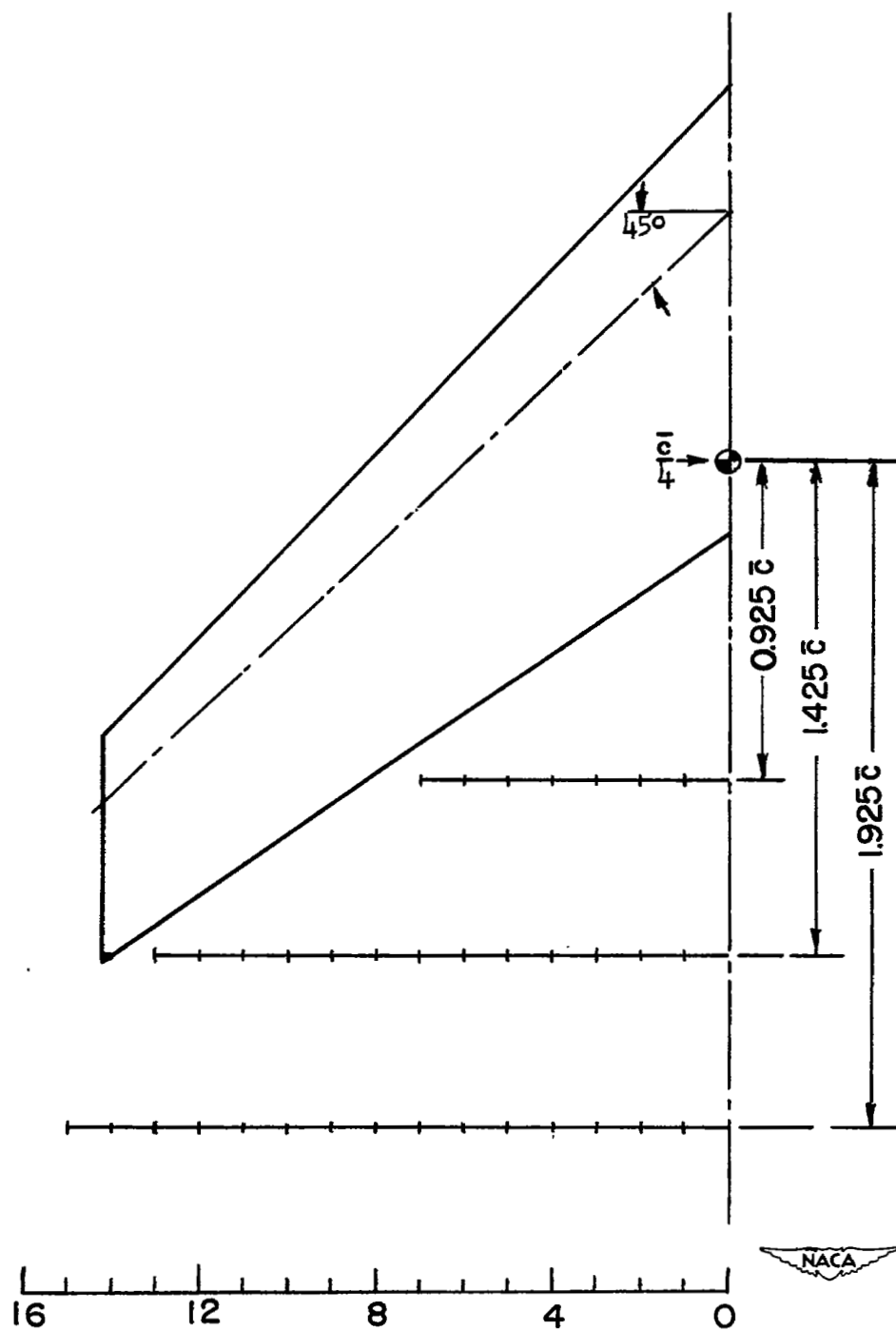
Lateral distance from plane of symmetry, ft

Figure 6.- Longitudinal locations of the three vertical survey planes.

○ Basic wing
▣ Drooped-nose flaps deflected 40°
◇ Drooped-nose and semispan plain flaps deflected 40°
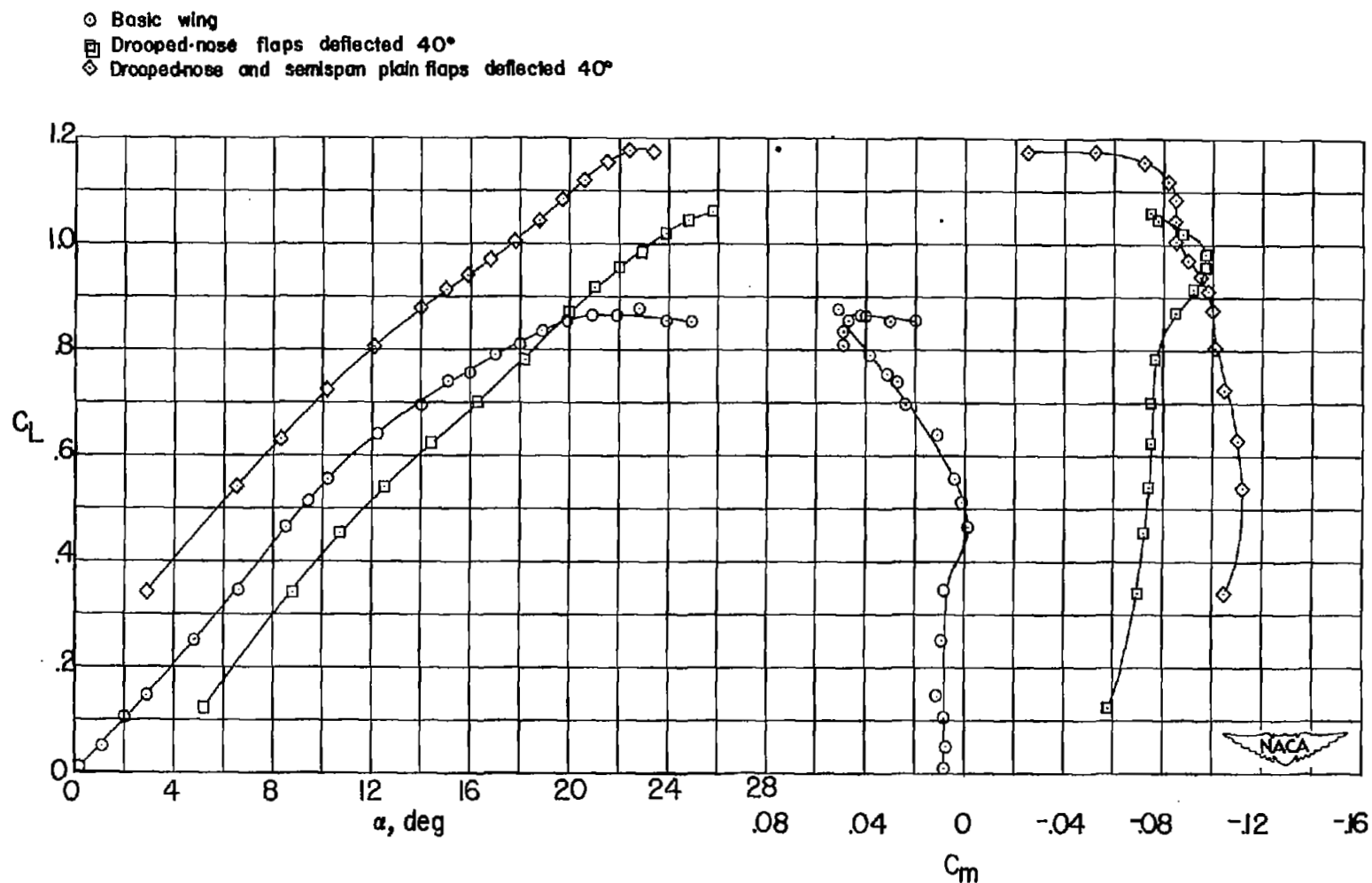
Figure 7.- Variation of lift coefficient with angle of attack for the
47.5° sweptback wing with flaps neutral and deflected. R ≈ 4.3 × 10^6.
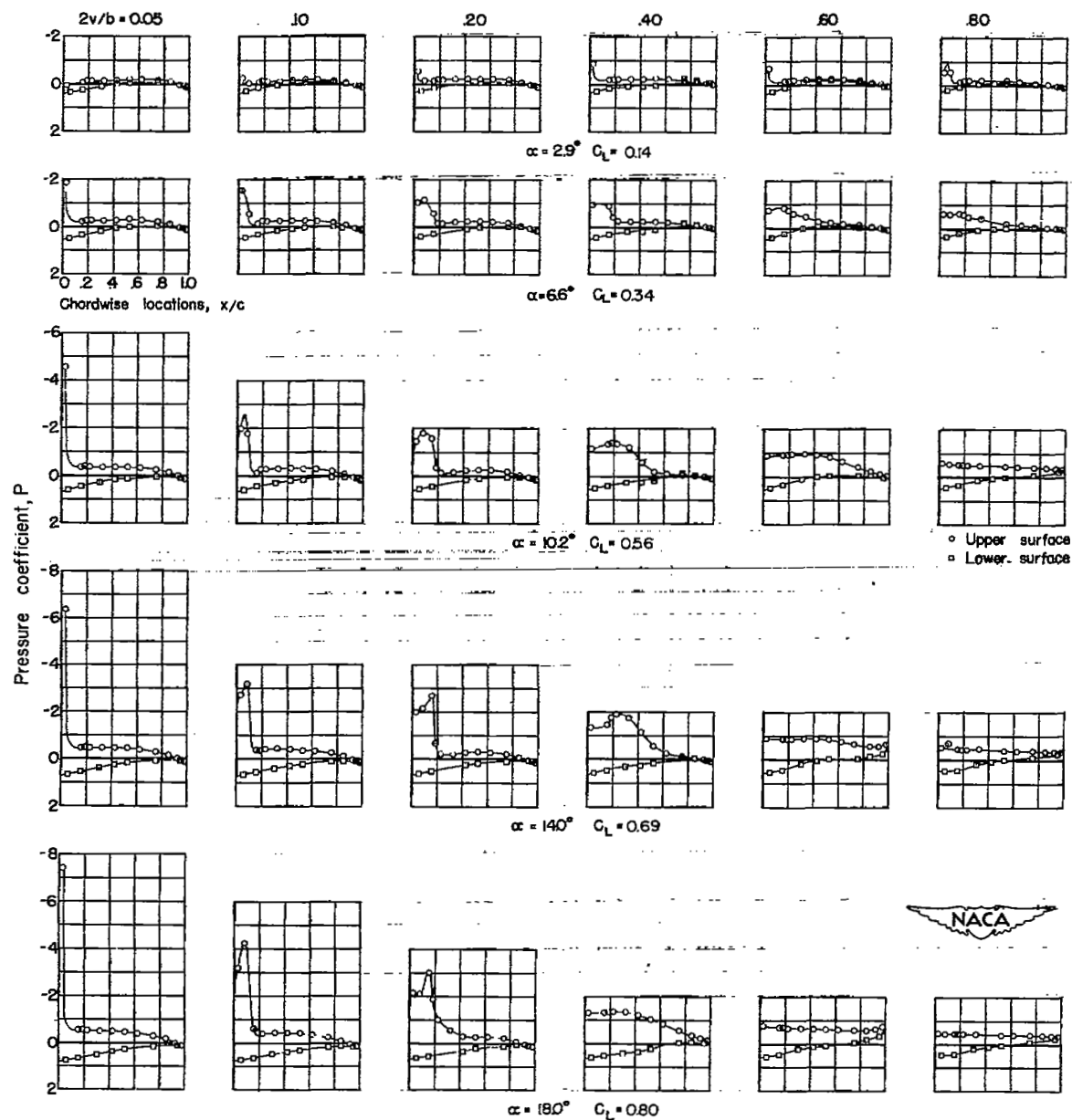
Figure 8.- Chordwise pressure distribution for six spanwise stations. Basic wing.
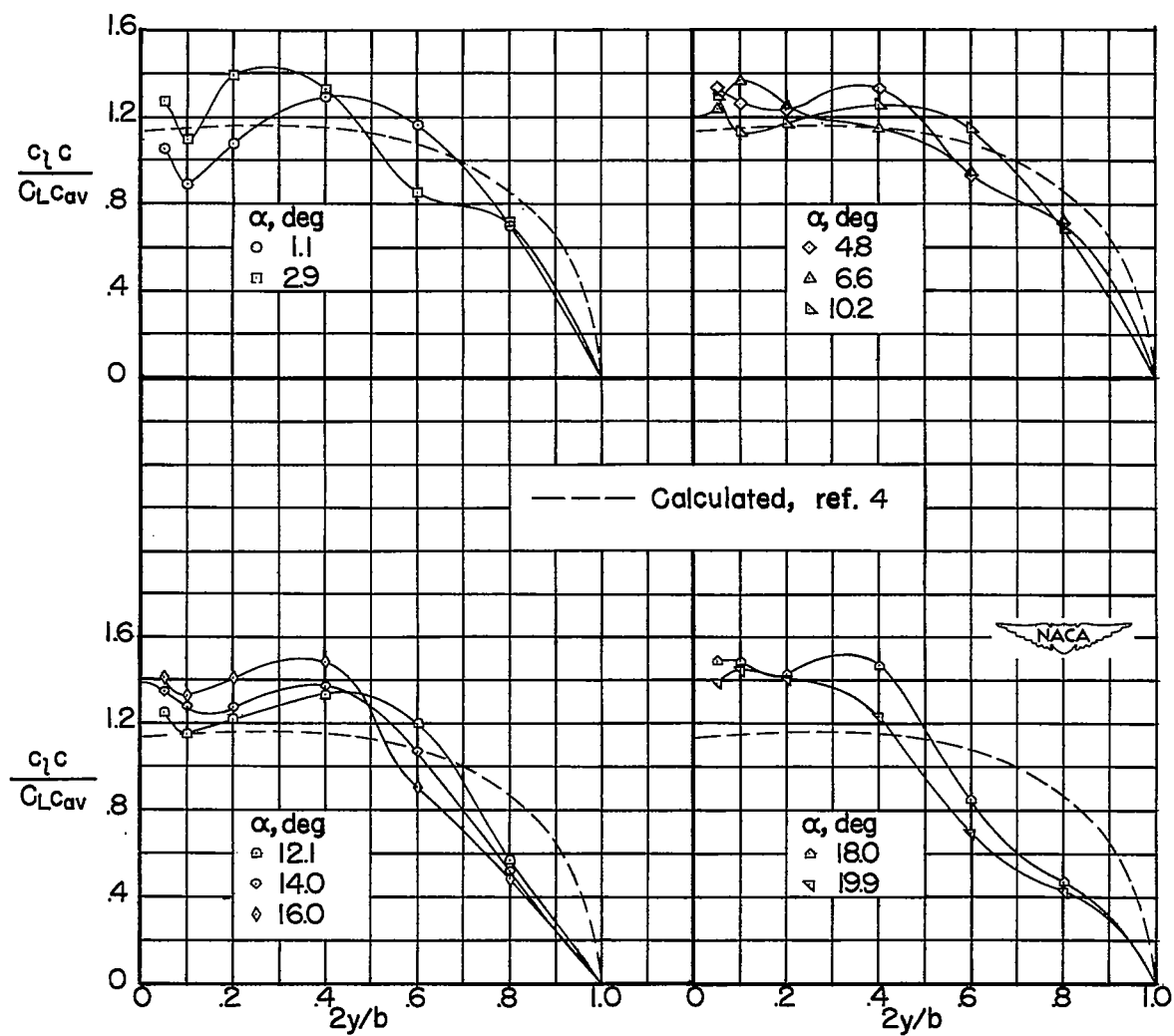
Figure 9.- Span load distribution for several angles of attack. Basic wing.
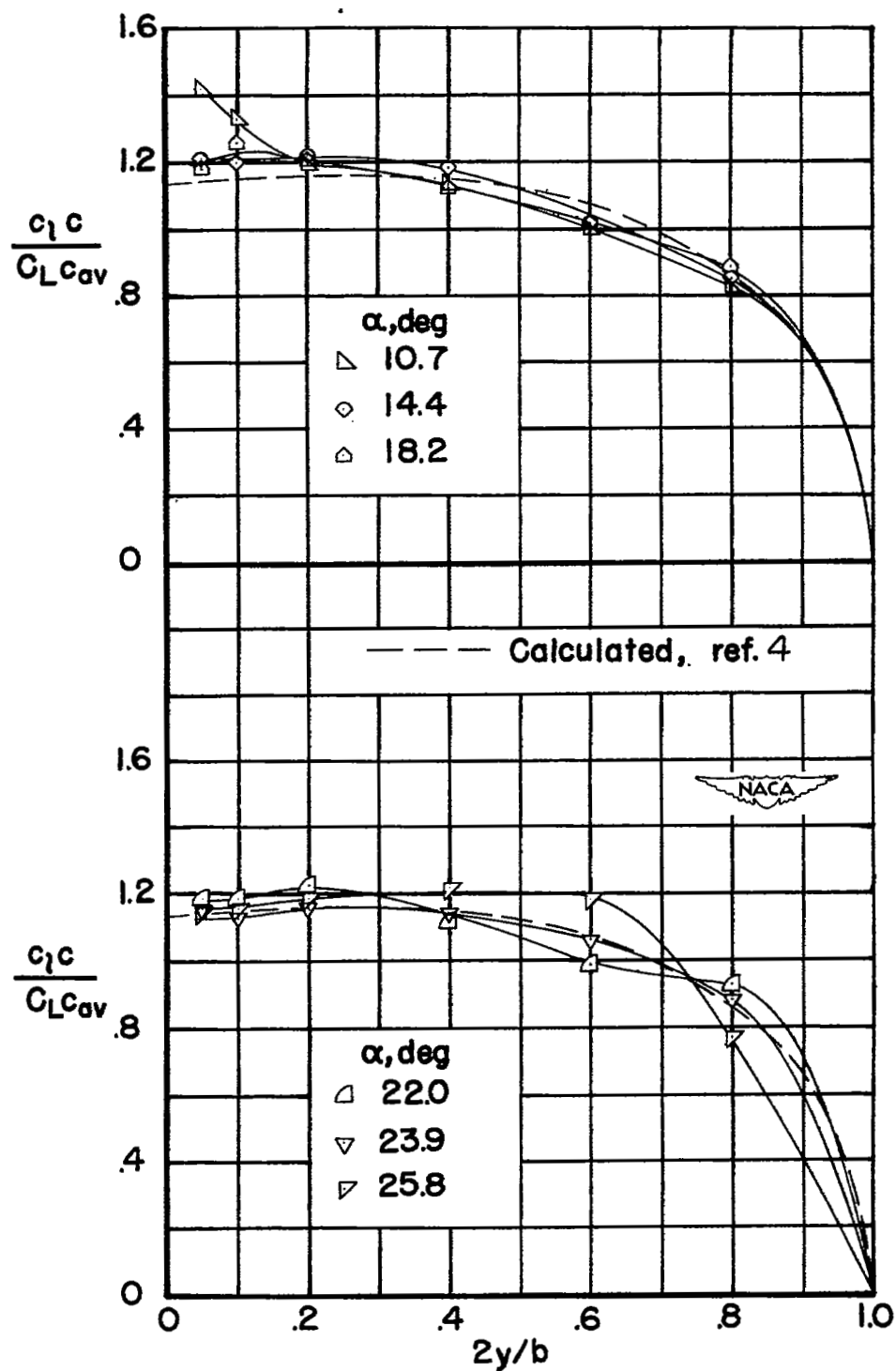
Figure 10.- Span load distribution for several angles of attack.
Drooped-nose flap deflected 40°.
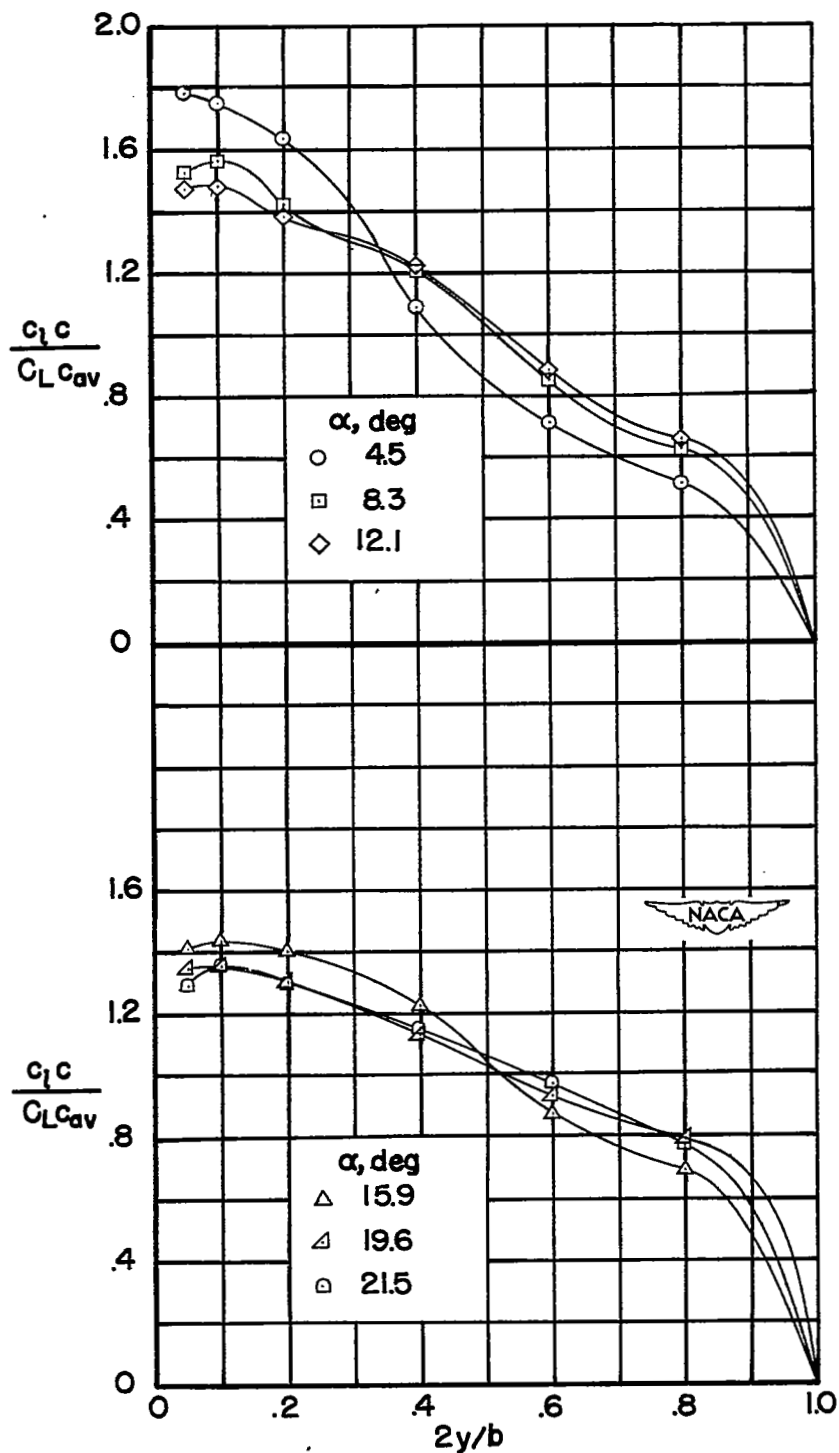
Figure 11.- Span load distribution for several angles of attack. Drooped-nose flap and semispan plain flap deflected 40°.

Scale of vectors
0 10 20 30

Downwash and sidewash angles. Vectors denote deviation of airflow from free-stream direction
in degrees.

Vertical distance from chord plane extended, ft

Vertical distance from chord plane extended, ft

15   14   13   12   11   10   9   8   7   6   5   4   3   2   1   0
Wing tip   Lateral distance from plane of symmetry, ft
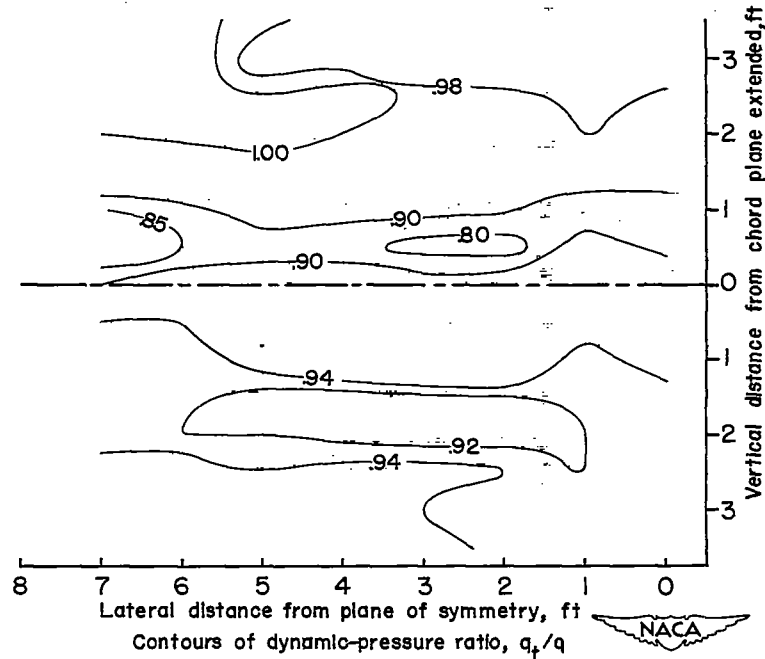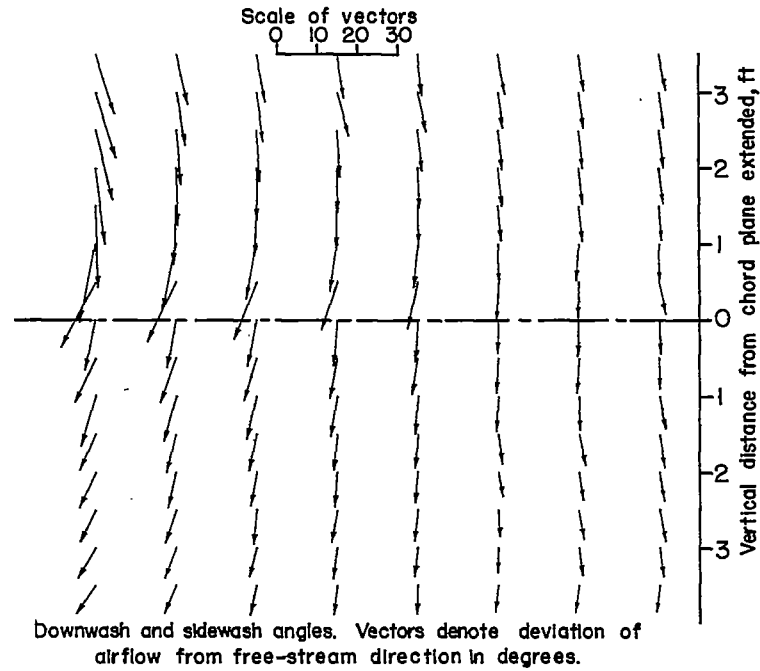   Contours of dynamic-pressure ratio, q_t/q
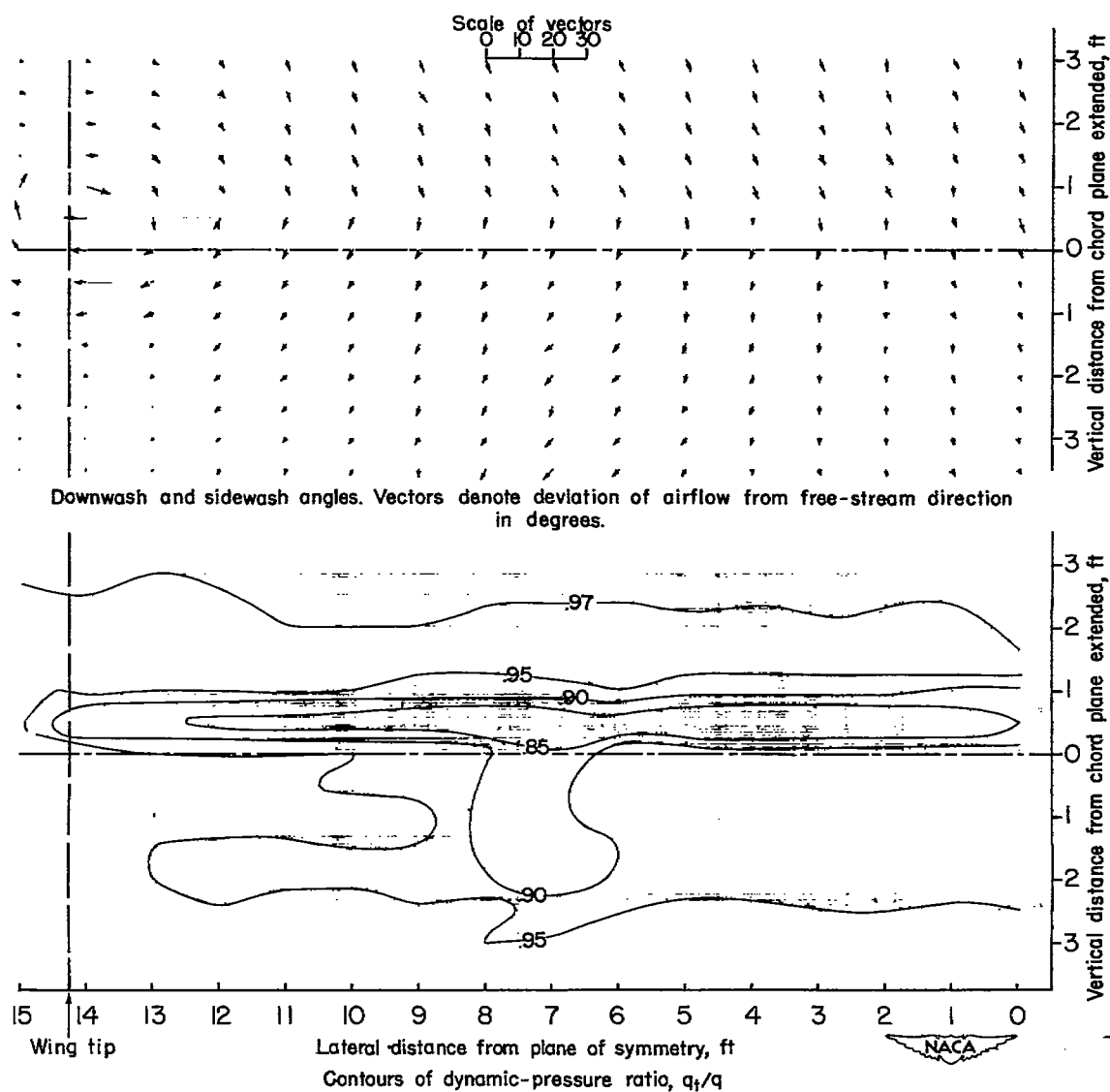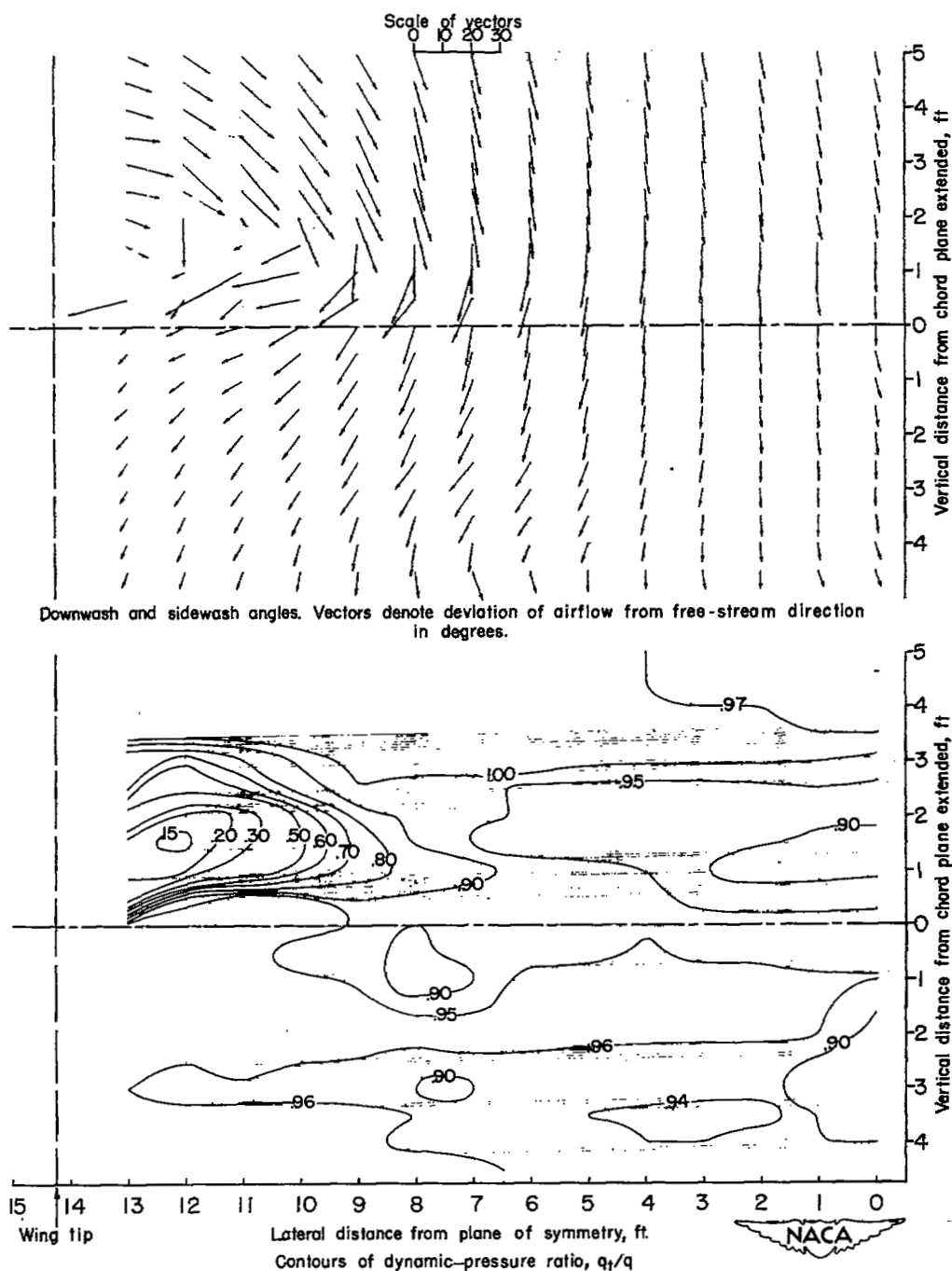
Figure 12.- Vectors of downwash and sidewash angle and contours of
   dynamic-pressure ratio behind a 47.5° sweptback wing. Longitudinal
   plane of survey at 1.925c̄. Basic wing configuration. α = 2.9°;
   C_L = 0.14.

Scale of vectors
0 10 20 30

Downwash and sidewash angles. Vectors denote deviation of airflow from free-stream
direction in degrees.

15 14 13 12 11 10 9 8 7 6 5 4 3 2 1 0
Wing tip   Lateral distance from plane of symmetry, ft
Contours of dynamic-pressure ratio, q_t/q
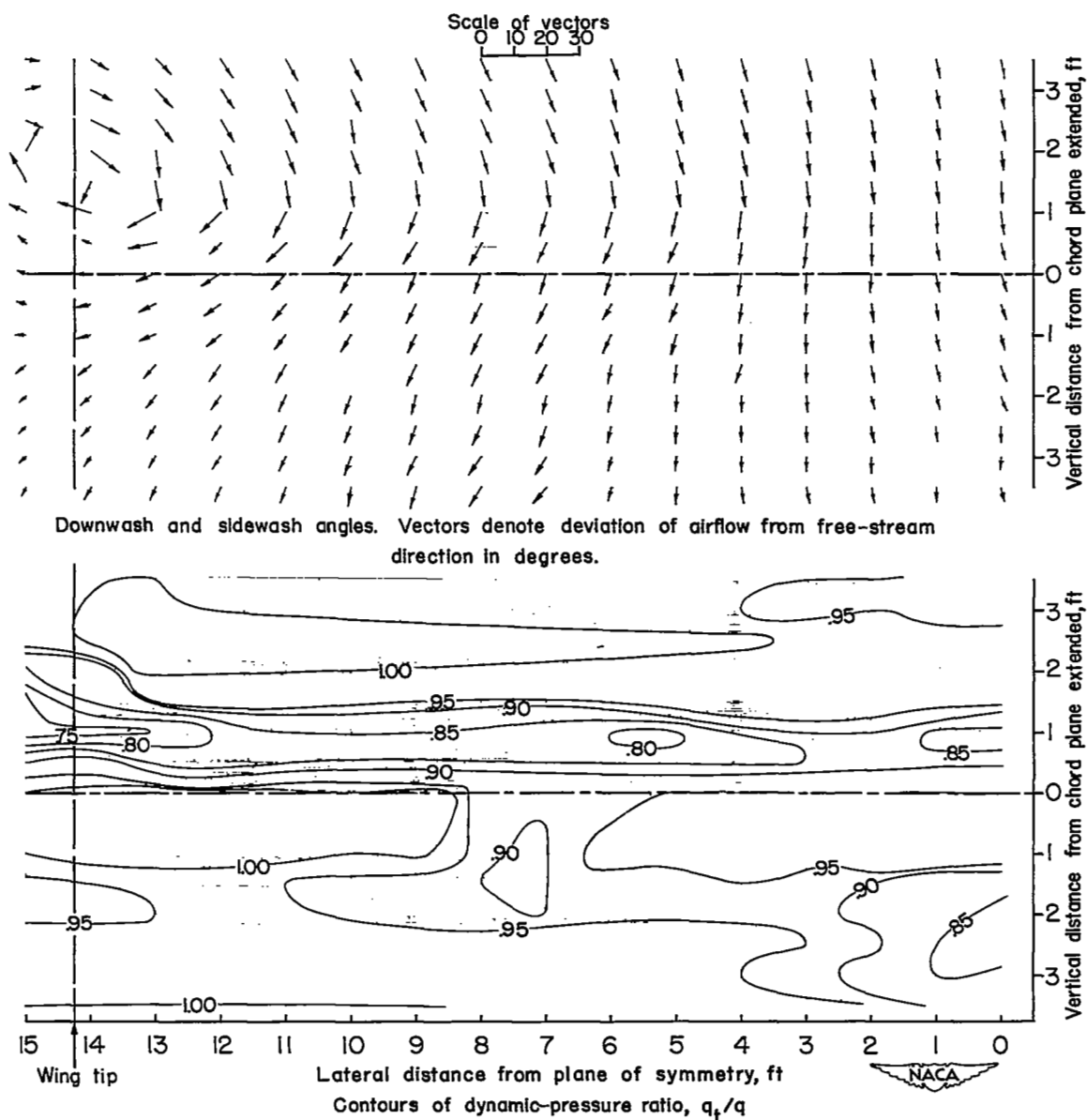
Figure 13.- Vectors of downwash and sidewash angle and contours of
dynamic-pressure ratio behind a 47.5° sweptback wing. Longitudinal
plane of survey at $1.925\bar{c}$. Basic wing configuration. $\alpha = 6.6^\circ$;
$C_L = 0.34$.

Scale of vectors
0 10 20 30

Downwash and sidewash. Vectors denote deviation of airflow from free-stream direction
in degrees.

Vertical distance from chord plane extended, ft

Vertical distance from chord plane extended ft

Wing tip

Lateral distance from plane of symmetry, ft

NACA

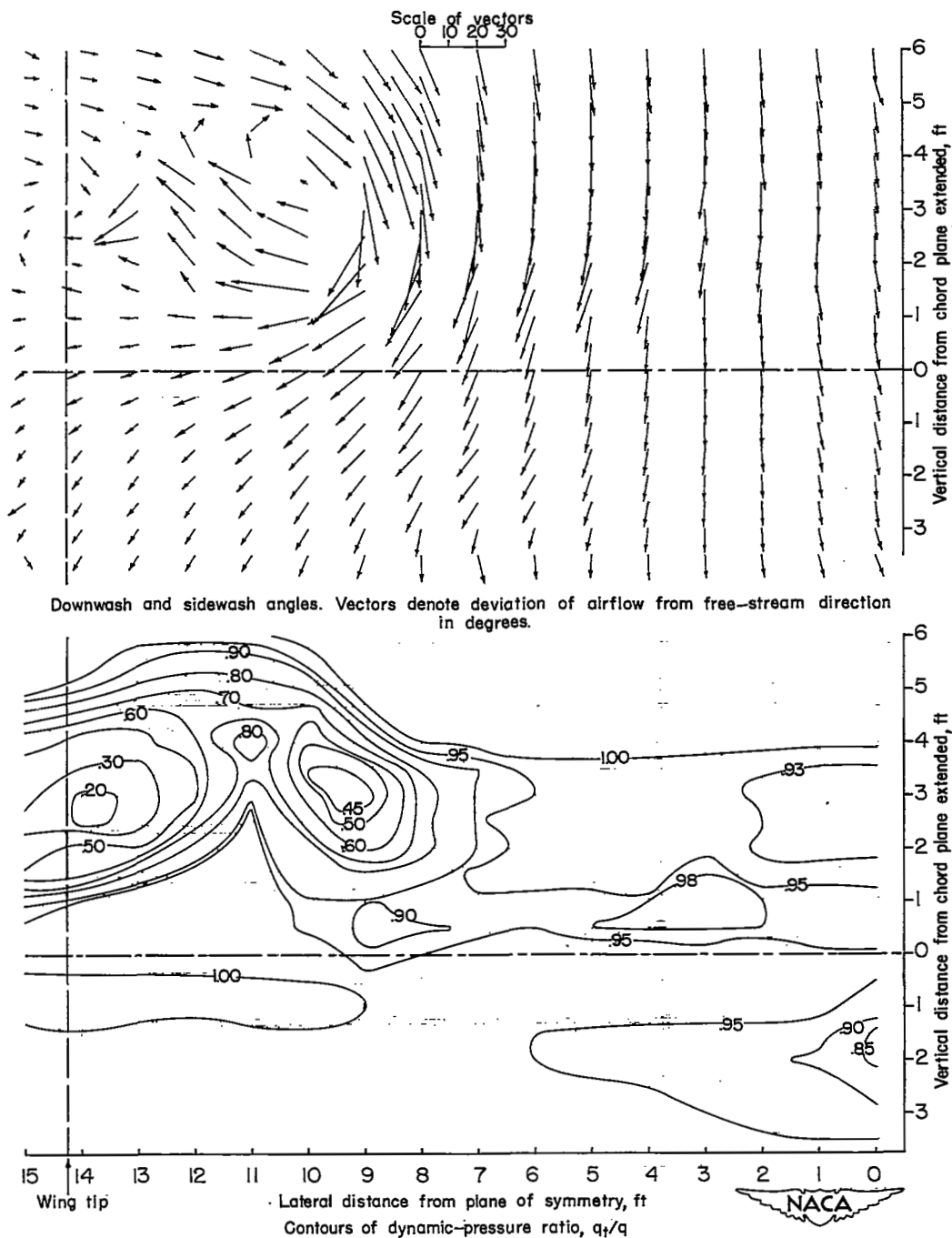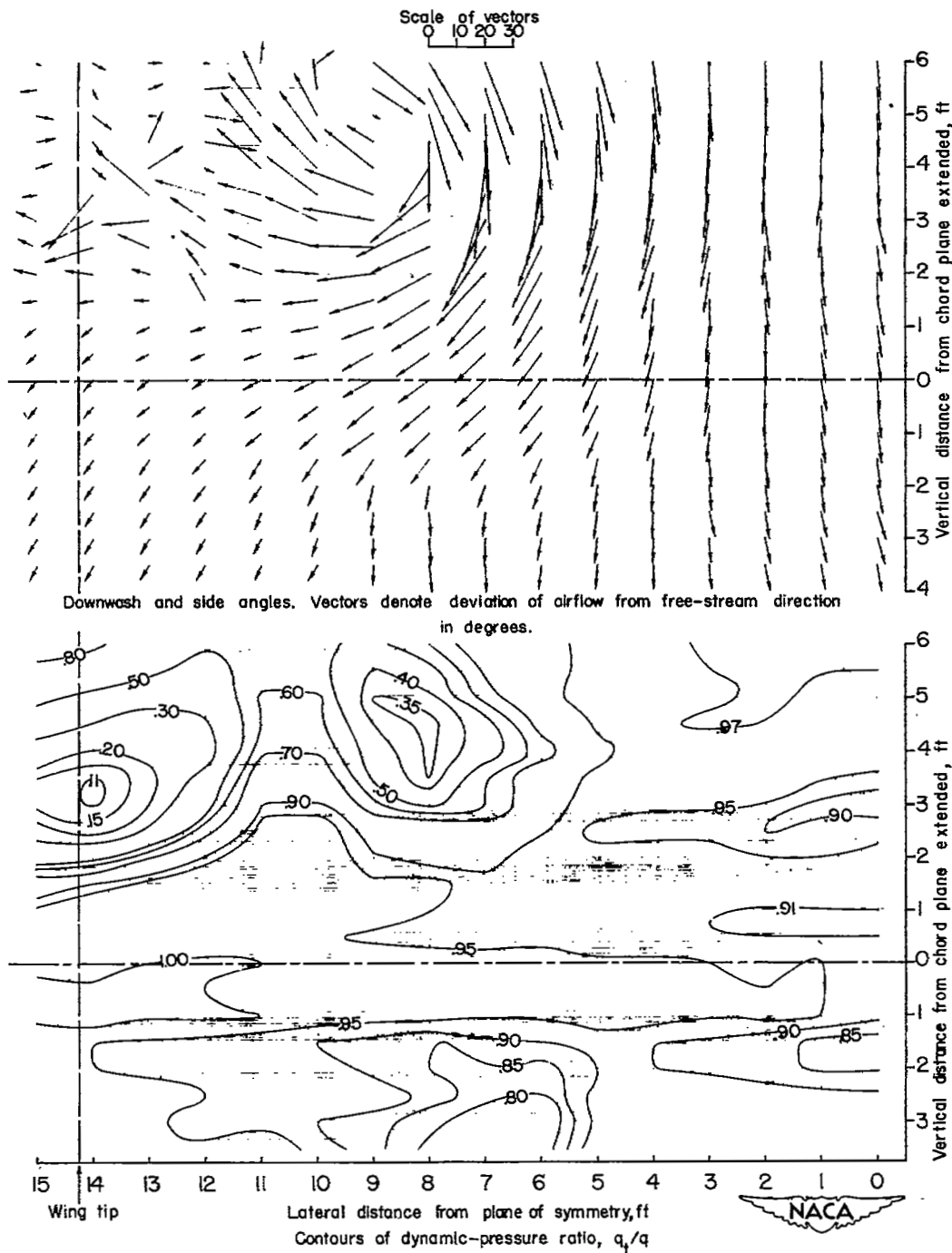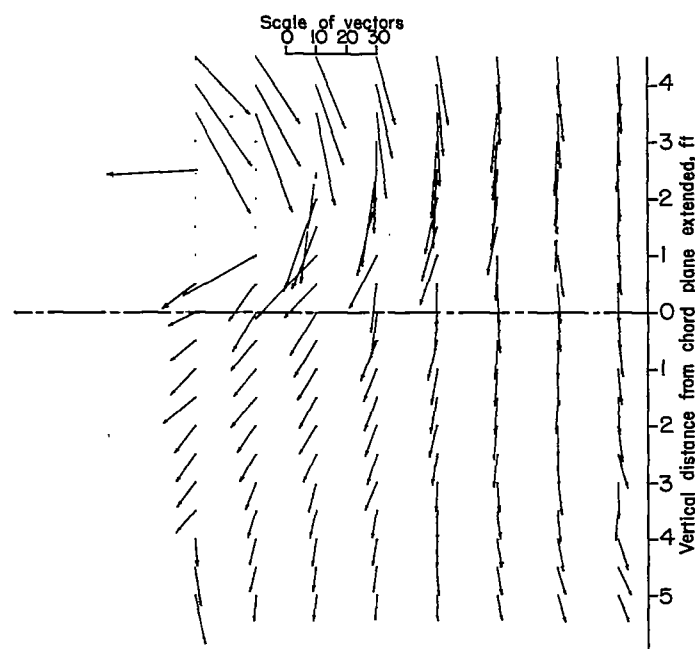Contours of dynamic-pressure ratio, q_t/q
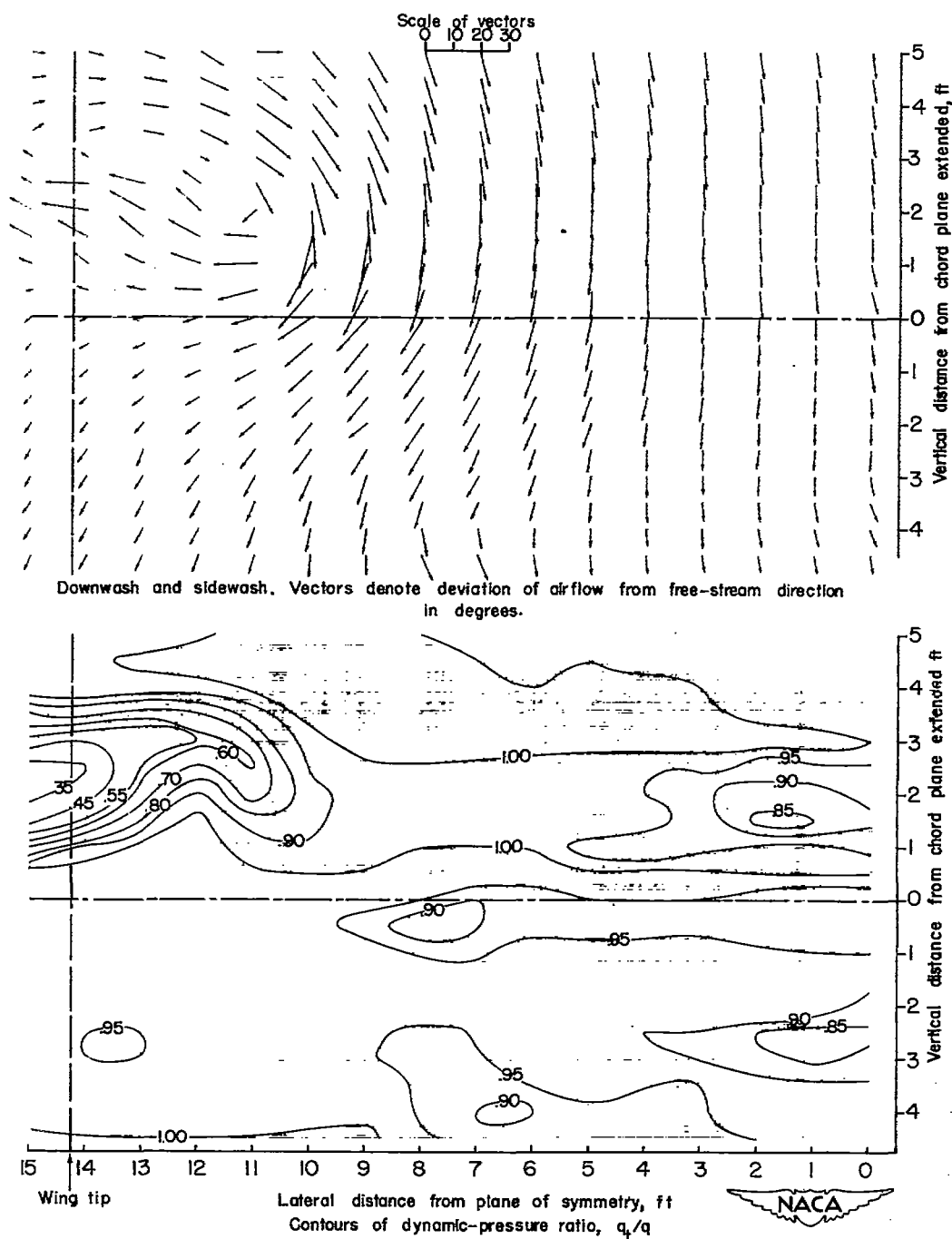
Figure 14.- Vectors of downwash and sidewash angle and contours of
dynamic-pressure ratio behind a 47.5° sweptback wing. Longitudinal
plane of survey at 1.925$\bar{c}$. Basic wing configuration. $\alpha = 10.2°$;
$C_L = 0.56$.

Scale of vectors
0 10 20 30

Downwash and sidewash angles. Vectors denote deviation of
airflow from free-stream direction in degrees.

Contours of dynamic-pressure ratio, q_t/q

Lateral distance from plane of symmetry, ft

Figure 15.- Vectors of downwash and sidewash angle and contours of
dynamic-pressure ratio behind a 47.5° sweptback wing. Longitudinal
plane of survey at $0.925\bar{c}$. Basic wing configuration. $\alpha = 10.2^{\circ}$;
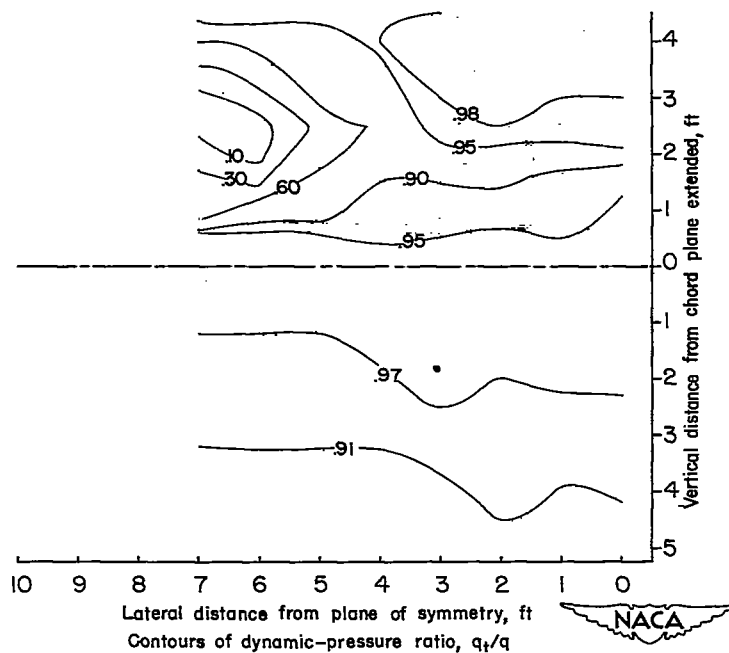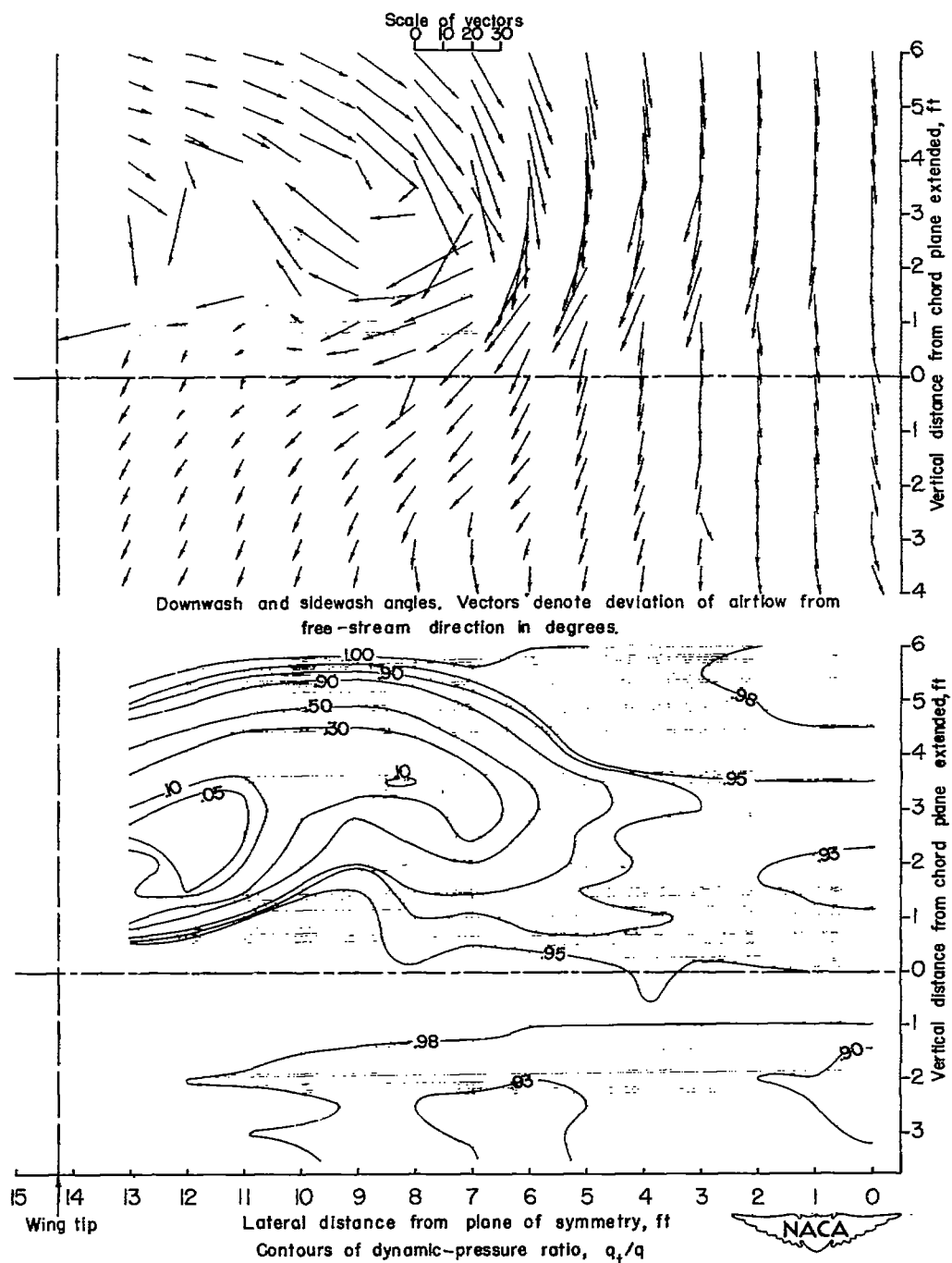$C_L = 0.56$.

Figure 16.- Vectors of downwash and sidewash angle and contours of dynamic-pressure ratio behind a 47.5° sweptback wing. Longitudinal plane of survey at 1.425c. Basic wing configuration. α = 10.2°; C_L = 0.56.

Scale of vectors
0 10 20 30

Downwash and sidewash angles. Vectors denote deviation of airflow from free—stream direction
in degrees.

Contours of dynamic—pressure ratio, q_t/q

Lateral distance from plane of symmetry, ft

Wing tip

Figure 17.- Vectors of downwash and sidewash angle and contours of dynamic-pressure ratio behind a 47.5° sweptback wing. Longitudinal plane of survey at $1.925\bar{c}$. Basic wing configuration. $\alpha = 14.0^\circ$; $C_T = 0.69$.

Scale of vectors
0 10 20 30

Downwash and side angles. Vectors denote deviation of airflow from free-stream direction
in degrees.

Wing tip
Lateral distance from plane of symmetry, ft
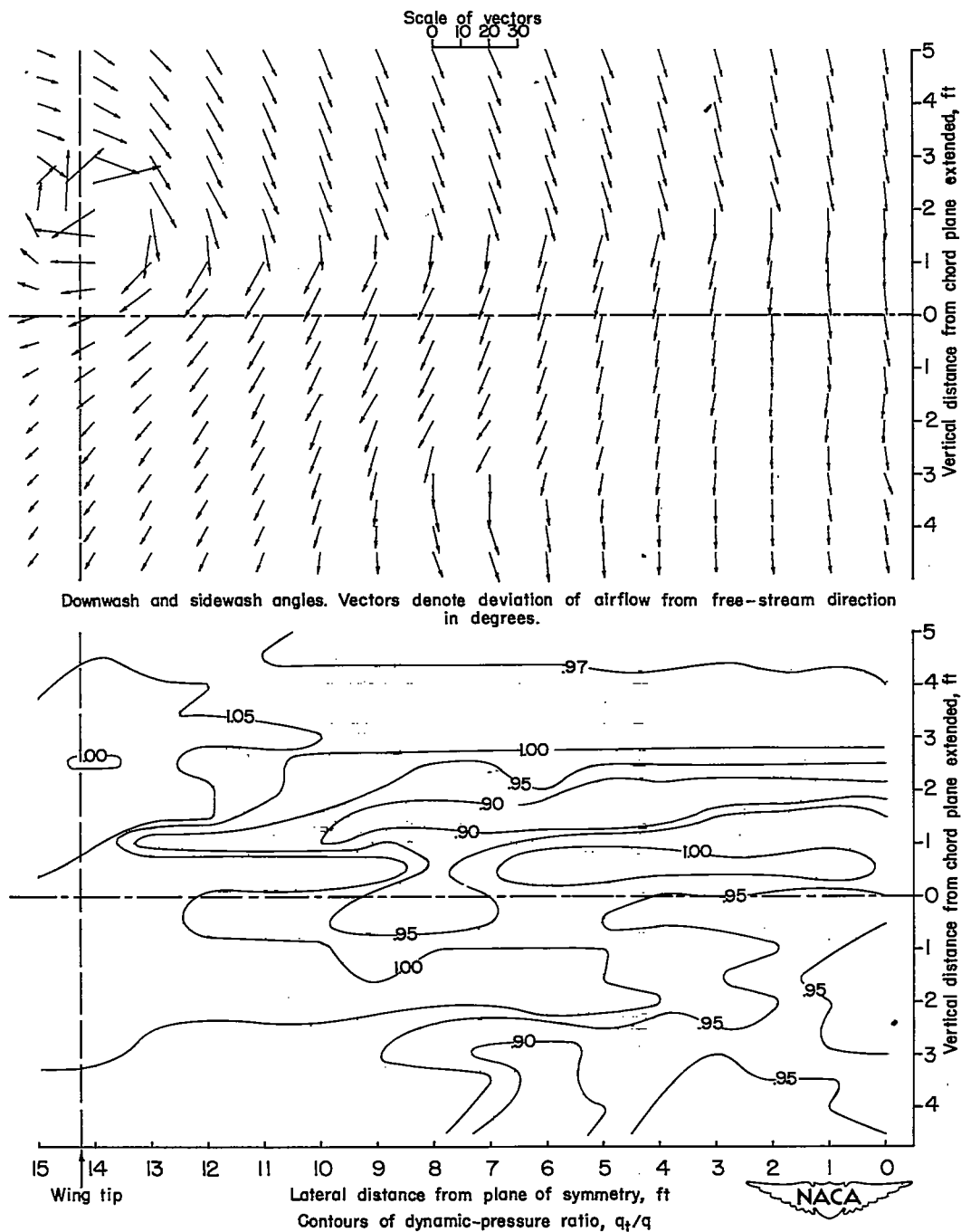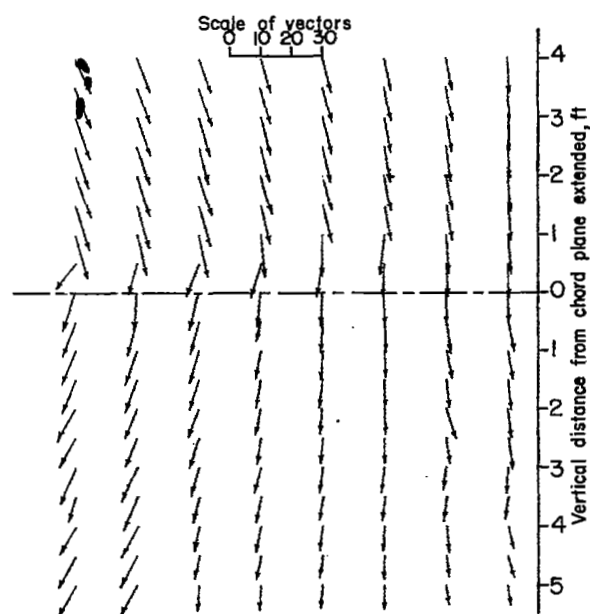Contours of dynamic-pressure ratio, q$_t$/q

Figure 18.- Vectors of downwash and sidewash angle and contours of
dynamic-pressure ratio behind a 47.5° sweptback wing. Longitudinal
plane of survey at 1.925c̄. Basic wing configuration. α = 18.0°;
C$_L$ = 0.80.

Scale of vectors
0 10 20 30

Downwash and sidewash angles. Vectors denote deviation of
airflow from free-stream direction in degrees.

Vertical distance from chord plane extended, ft

Vertical distance from chord plane extended, ft

Lateral distance from plane of symmetry, ft
Contours of dynamic-pressure ratio, q_t/q

NACA

Figure 19.- Vectors of downwash and sidewash angle and contours of
dynamic-pressure ratio behind a 47.5° sweptback wing. Longitudinal
plane of survey at $0.925\bar{c}$. Basic wing configuration. $\alpha = 18.0^{\circ}$;
$C_L = 0.80$.

Figure 20.— Vectors of downwash and sidewash angle and contours of dynamic-pressure ratio behind a 47.5° sweptback wing. Longitudinal plane of survey at 1.425c̄. Basic wing configuration. $\alpha = 18.0^{\circ}$; $C_L = 0.80$.
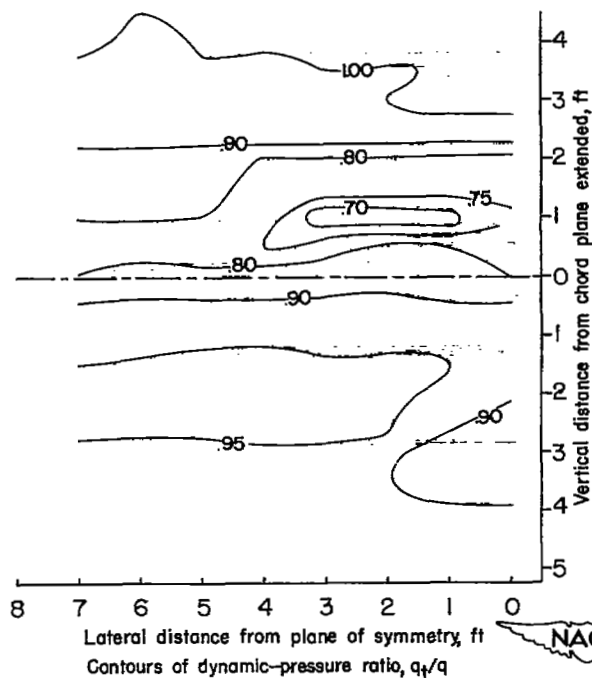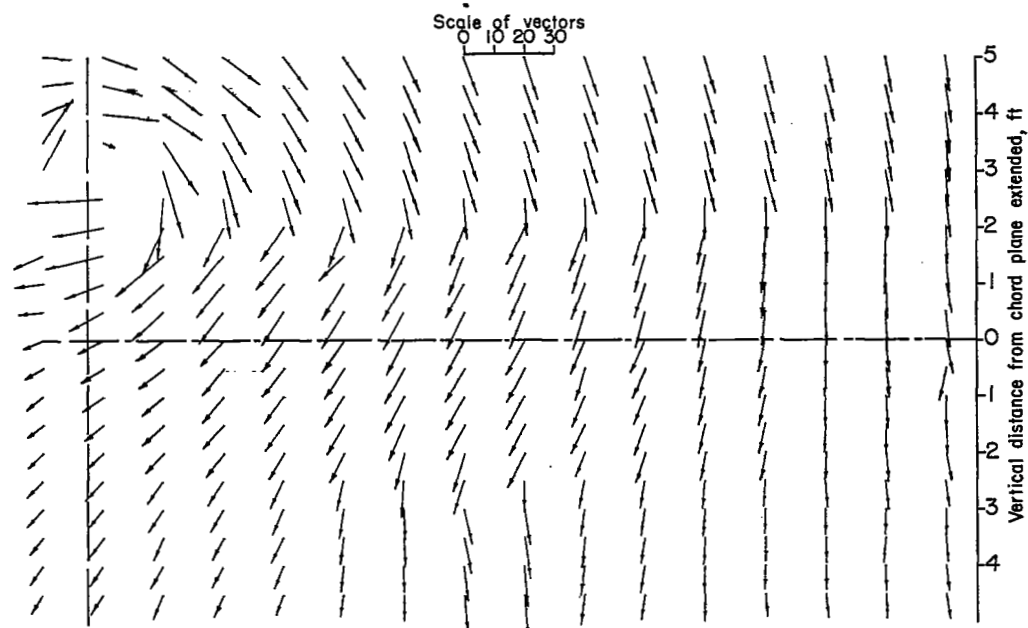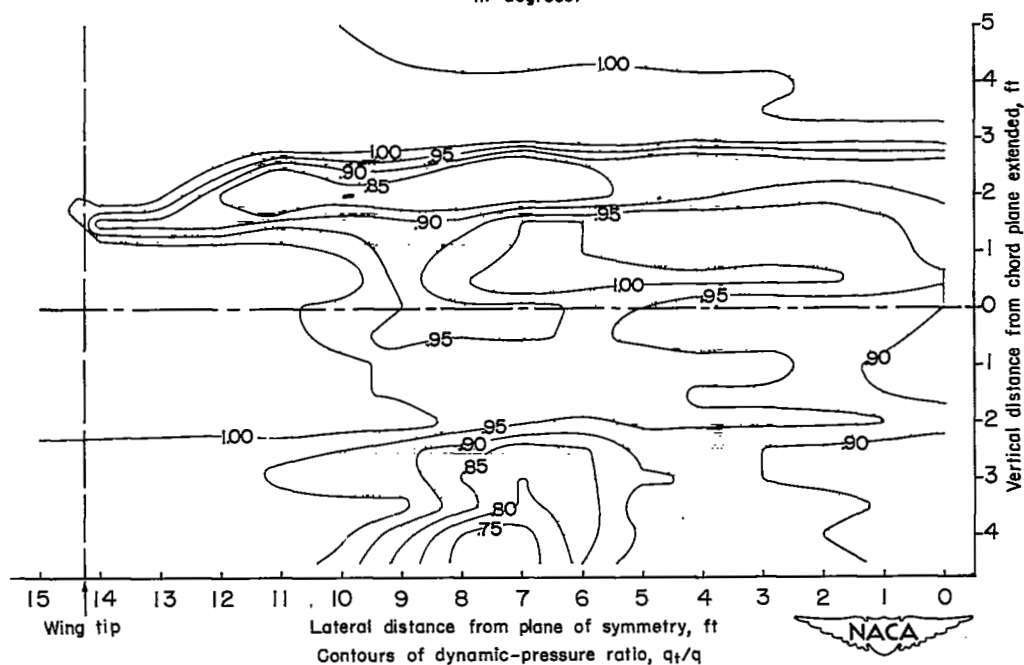
Figure 21.- Vectors of downwash and sidewash angle and contours of dynamic-pressure ratio behind a 47.5° sweptback wing. Longitudinal plane of survey at 1.925c̄. Drooped-nose flaps deflected 40°. α = 14.4°; C_L = 0.62.

Scale of vectors
0 10 20 30

Downwash and sidewash angles. Vectors denote deviation of airflow from free-stream direction in degrees.

Contours of dynamic-pressure ratio, q_t/q
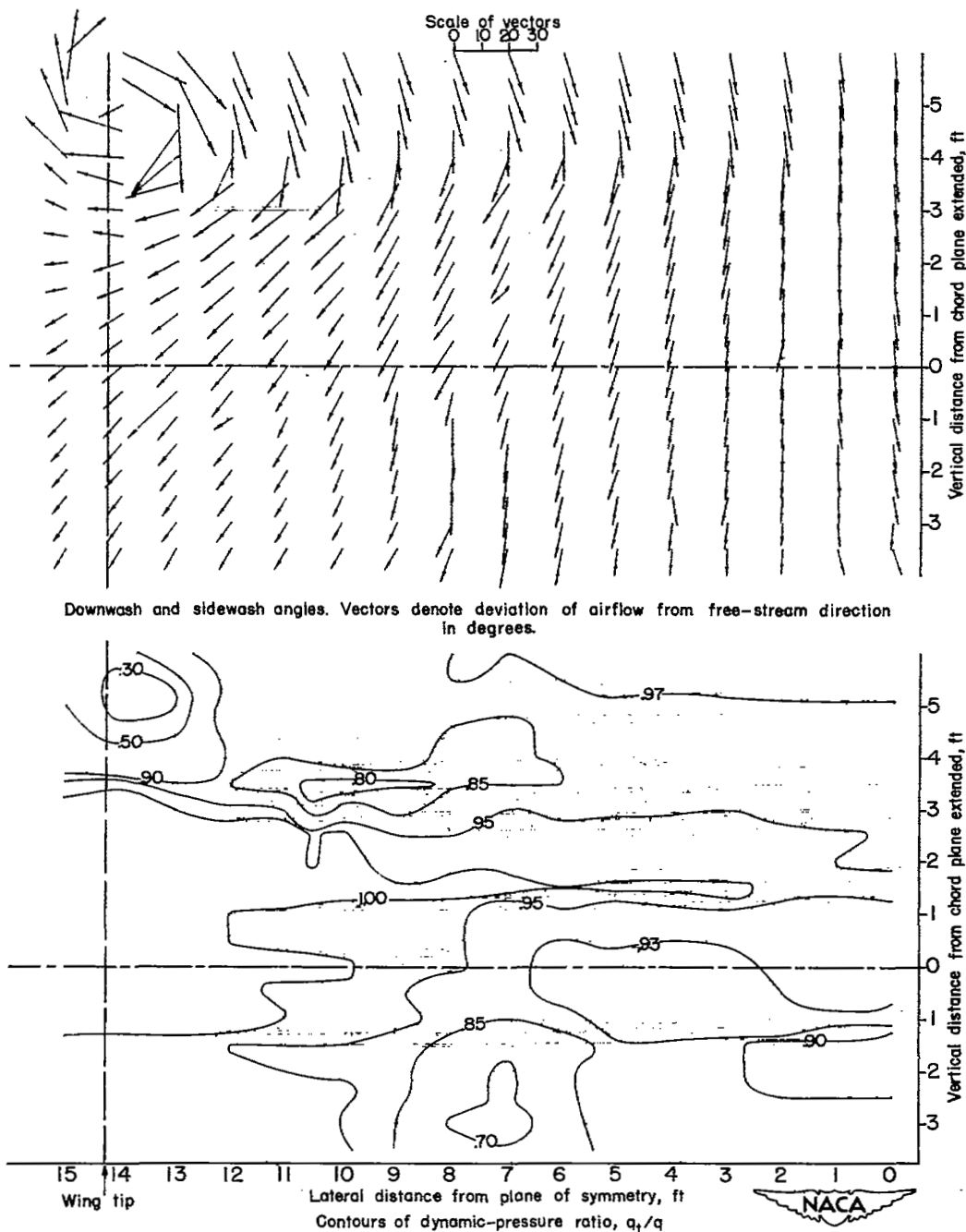
Lateral distance from plane of symmetry, ft

Figure 22.- Vectors of downwash and sidewash angle and contours of dynamic-pressure ratio behind a 47.5° sweptback wing. Longitudinal plane of survey at 0.925c. Drooped-nose flaps deflected 40°. $\alpha = 14.4°$; $C_L = 0.62$.

Scale of vectors
0 10 20 30

Downwash and sidewash angles. Vectors denote deviation of airflow from free—stream direction in degrees.

Vertical distance from chord plane extended, ft

Vertical distance from chord plane extended, ft

15   14   13   12   11   10   9   8   7   6   5   4   3   2   1   0

Wing tip   Lateral distance from plane of symmetry, ft

NACA
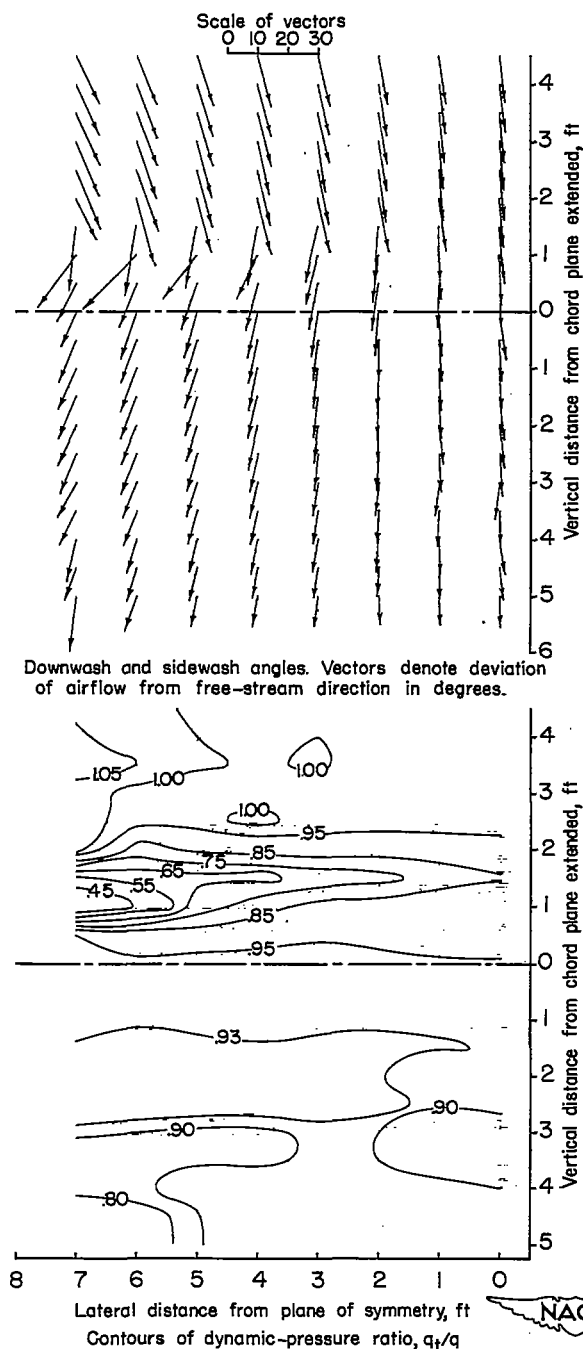
Contours of dynamic-pressure ratio, q_t/q

Figure 23.- Vectors of downwash and sidewash angle and contours of dynamic-pressure ratio behind a 47.5^O sweptback wing. Longitudinal plane of survey at $1.925\bar{c}$. Drooped-nose flaps deflected 40°. $\alpha = 18.2^O$; $C_L = 0.78$.

Scale of vectors
0 10 20 30

Downwash and sidewash angles. Vectors denote deviation of airflow from free-stream direction
in degrees.

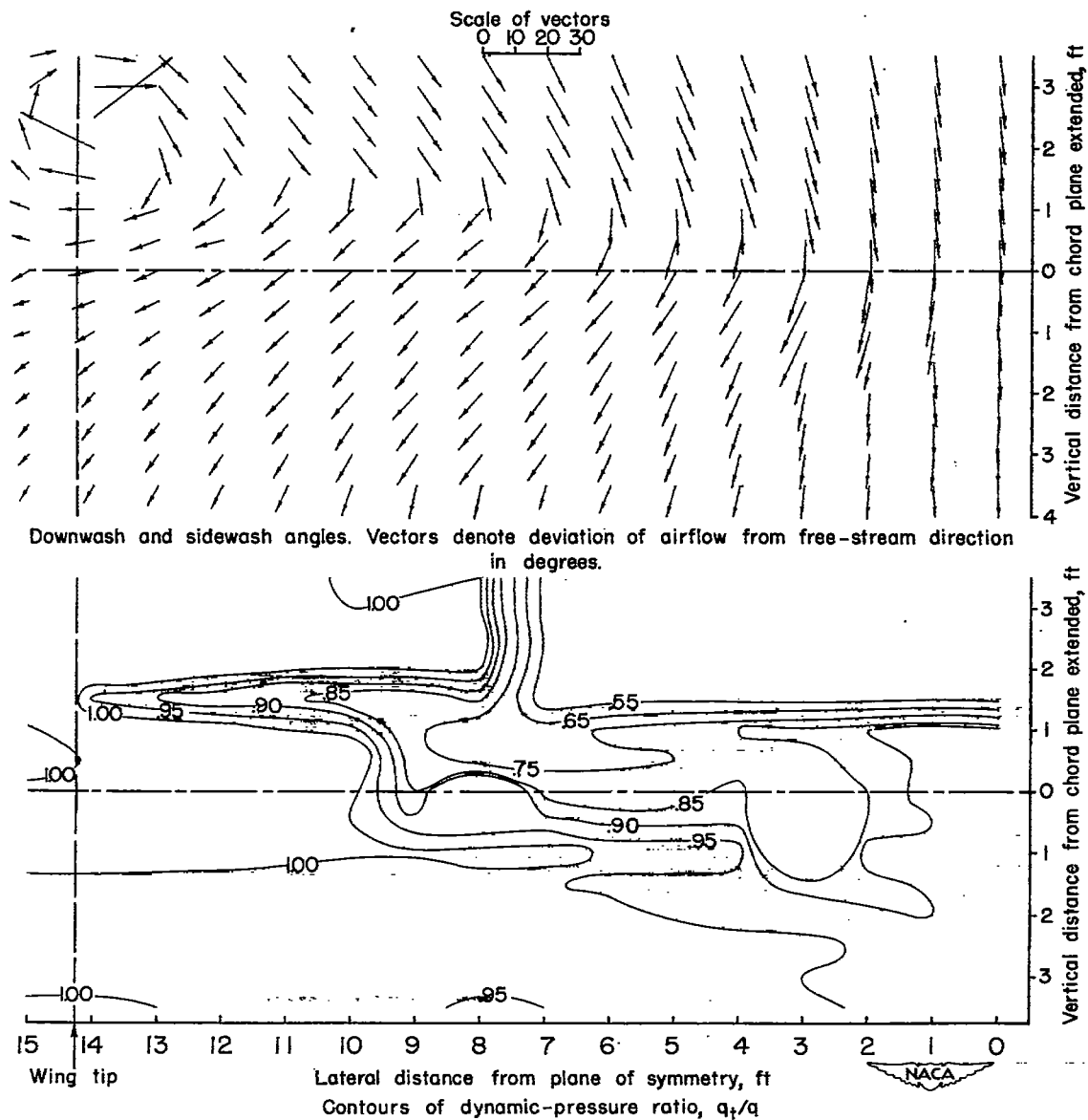Contours of dynamic-pressure ratio, q_1/q

NACA

Figure 24.- Vectors of downwash and sidewash angle and contours of dynamic-pressure ratio behind a 47.5° sweptback wing. Longitudinal plane of survey at 1.925c̄. Drooped-nose flaps deflected 40°. α = 22.0°; C_L = 0.96.

Scale of vectors
0 10 20 30

Downwash and sidewash angles. Vectors denote deviation
of airflow from free-stream direction in degrees.

Lateral distance from plane of symmetry, ft
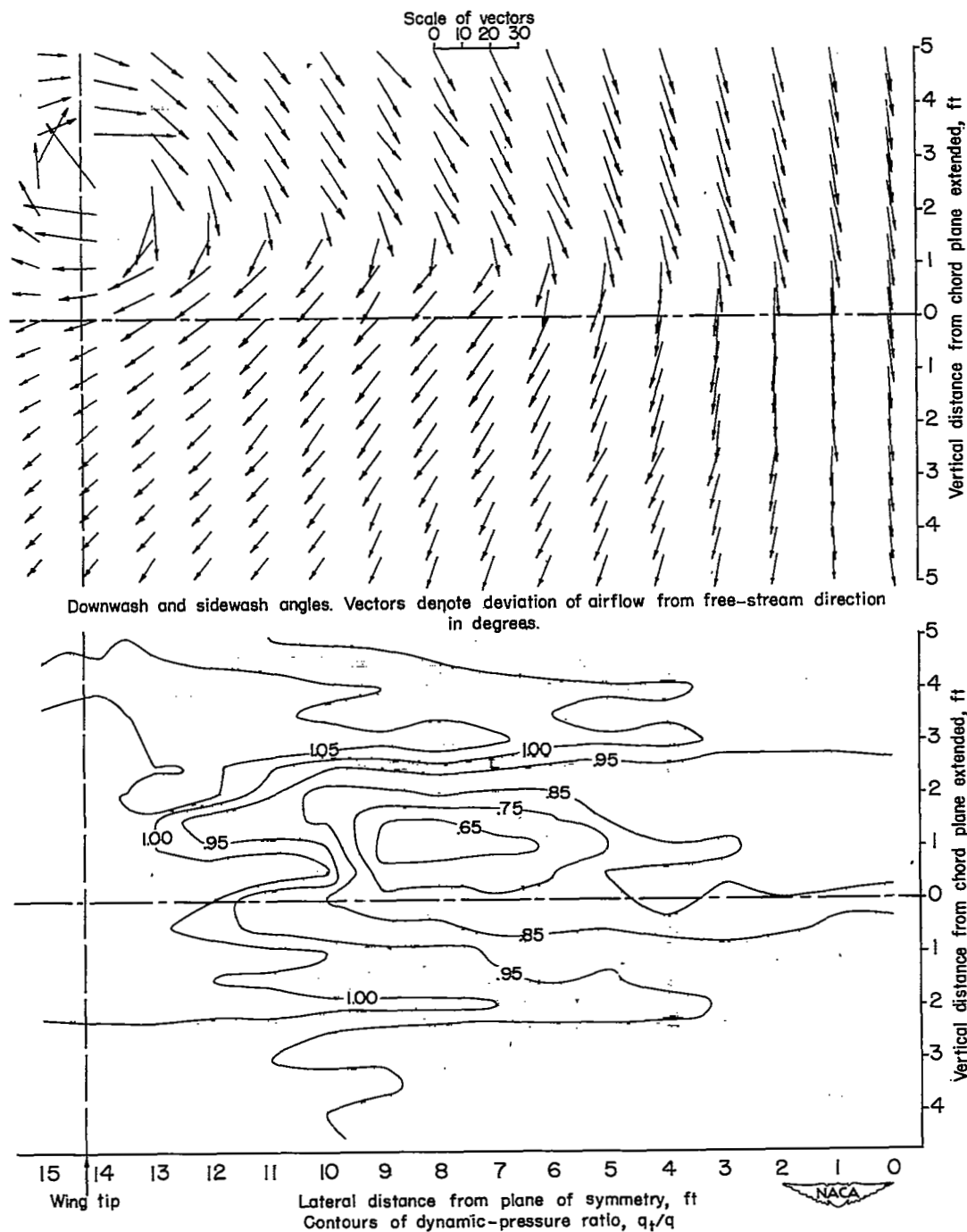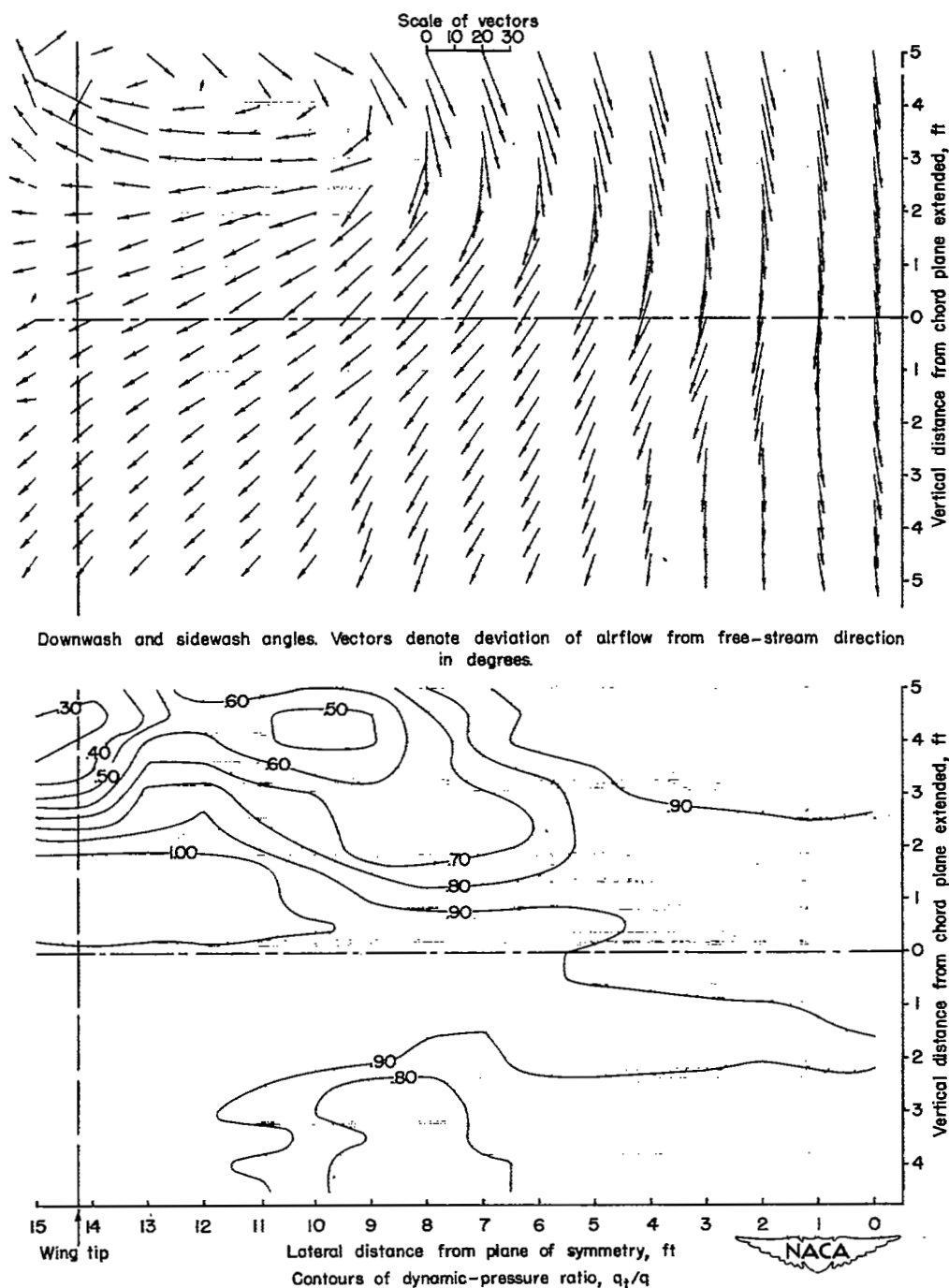
Contours of dynamic-pressure ratio, q_t/q

Figure 25.- Vectors of downwash and sidewash angle and contours of
dynamic-pressure ratio behind a 47.5^o sweptback wing. Longitudinal
plane of survey at $0.925\bar{c}$. Drooped-nose flaps deflected 40°.
$\alpha = 22.0^o$; $C_L = 0.96$.

Scale of vectors
0 10 20 30

Downwash and sidewash angles. Vectors denote deviation of airflow from free-stream direction in degrees.

Contours of dynamic-pressure ratio, q_t/q

Wing tip   Lateral distance from plane of symmetry, ft

Figure 26.- Vectors of downwash and sidewash angle and contours of dynamic-pressure ratio behind a 47.5° sweptback wing. Longitudinal plane of survey at $-1.925\bar{c}$. Drooped-nose flaps and semispan plain flaps deflected 40°. $\alpha = 8.3^\circ$; $C_L = 0.63$.
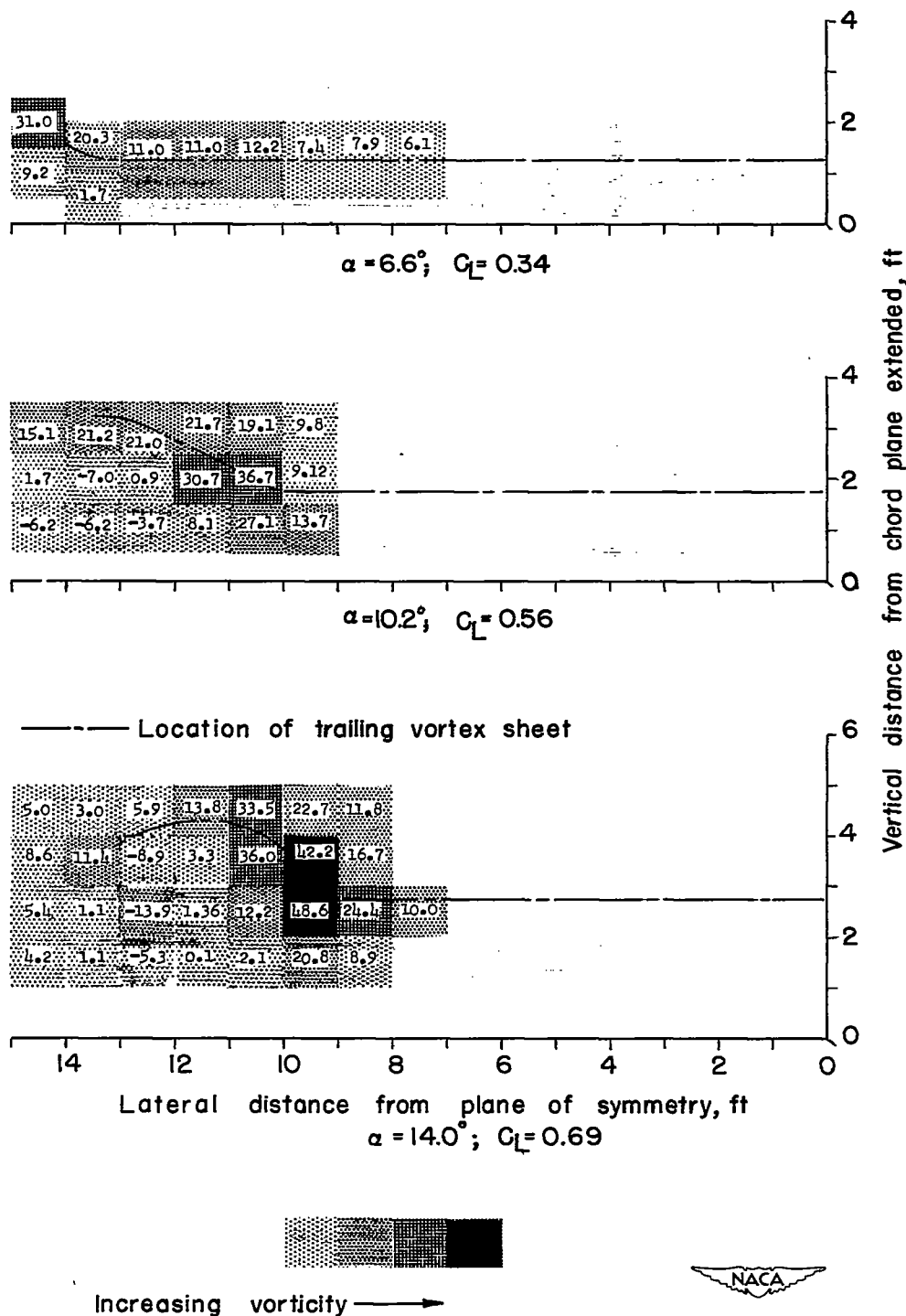
Scale of vectors
0 10 20 30

Downwash and sidewash angles. Vectors denote deviation of airflow from free-stream direction in degrees.

Vertical distance from chord plane extended, ft

Vertical distance from chord plane extended, ft

15 14 13 12 11 10 9 8 7 6 5 4 3 2 1 0

Wing tip

Lateral distance from plane of symmetry, ft
Contours of dynamic-pressure ratio, q_t/q

Figure 27.- Vectors of downwash and sidewash angle and contours of dynamic-pressure ratio behind a 47.5° sweptback wing. Longitudinal plane of survey at 1.925č. Drooped-nose flaps and semispan plain flaps deflected 40°. $\alpha = 15.9°$; $C_L = 0.94$.

Scale of vectors
0 10 20 30

Vertical distance from chord plane extended, ft

Downwash and sidewash angles. Vectors denote deviation of airflow from free-stream direction in degrees.

Vertical distance from chord plane extended, ft

15   14   13   12   11   10   9   8   7   6   5   4   3   2   1   0
Wing tip   Lateral distance from plane of symmetry, ft

Contours of dynamic-pressure ratio, q_t/q

Figure 28.- Vectors of downwash and sidewash angle and contours of dynamic-pressure ratio behind a 47.5° sweptback wing. Longitudinal plane of survey at $1.925\bar{c}$. Drooped-nose flaps and semispan plain flaps deflected 40°. $\alpha = 21.5^\circ$; $C_L = 1.15$.

$\alpha = 6.6°; \quad C_L = 0.34$

$\alpha = 10.2°; \quad C_L = 0.56$

——·—— Location of trailing vortex sheet

$\alpha = 14.0°; \quad C_L = 0.69$

Lateral distance from plane of symmetry, ft

Increasing vorticity ——➤

Figure 29.- Distribution of vorticity behind 47.5° sweptback wing with flaps neutral. Longitudinal location, 1.925c̄. The numbers in the hatched blocks represent the value of Γ.
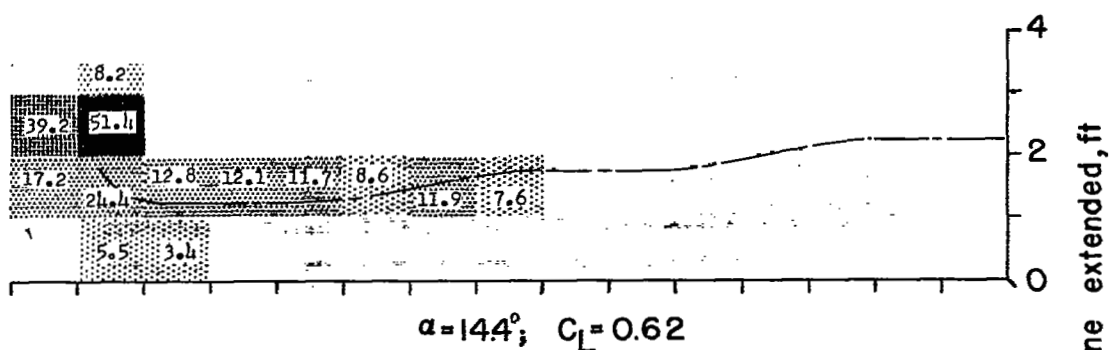
$\alpha = 14.4°$; $C_L = 0.62$

(a) Drooped-nose flaps deflected 40°.

————— Location of trailing vortex sheet

Lateral distance from plane of symmetry, ft

$\alpha = 15.9°$; $C_L = 0.94$
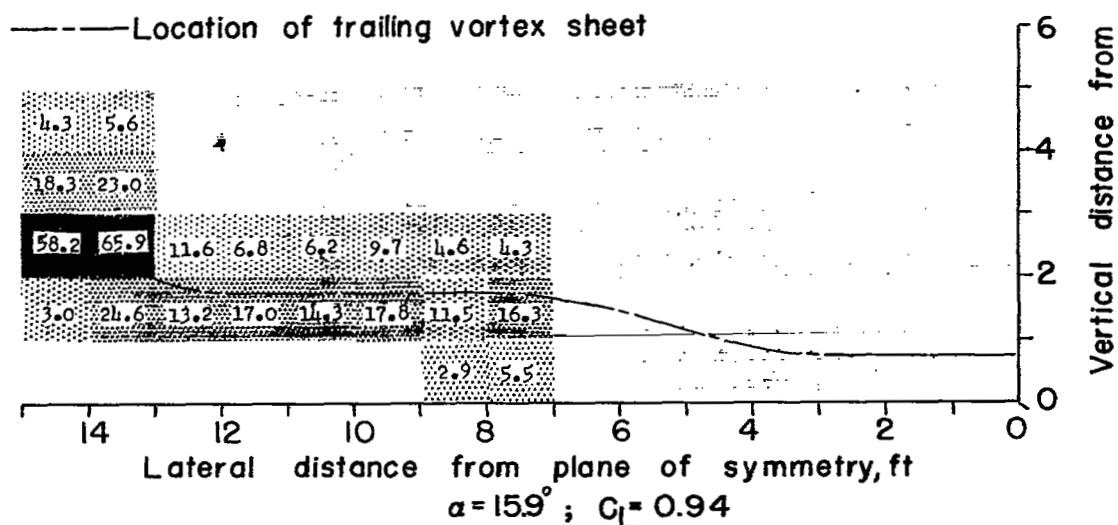
(b) Drooped-nose flaps and semispan plain flaps deflected 40°.

Increasing vorticity ⟶

Figure 30.- Distribution of vorticity behind 47.5° sweptback wing with flaps deflected. Longitudinal location, 1.925c̄. The numbers in the hatched blocks represent the value of Γ.

2.06 c̄

45°

16   12   8   4   0

Lateral distance, ft
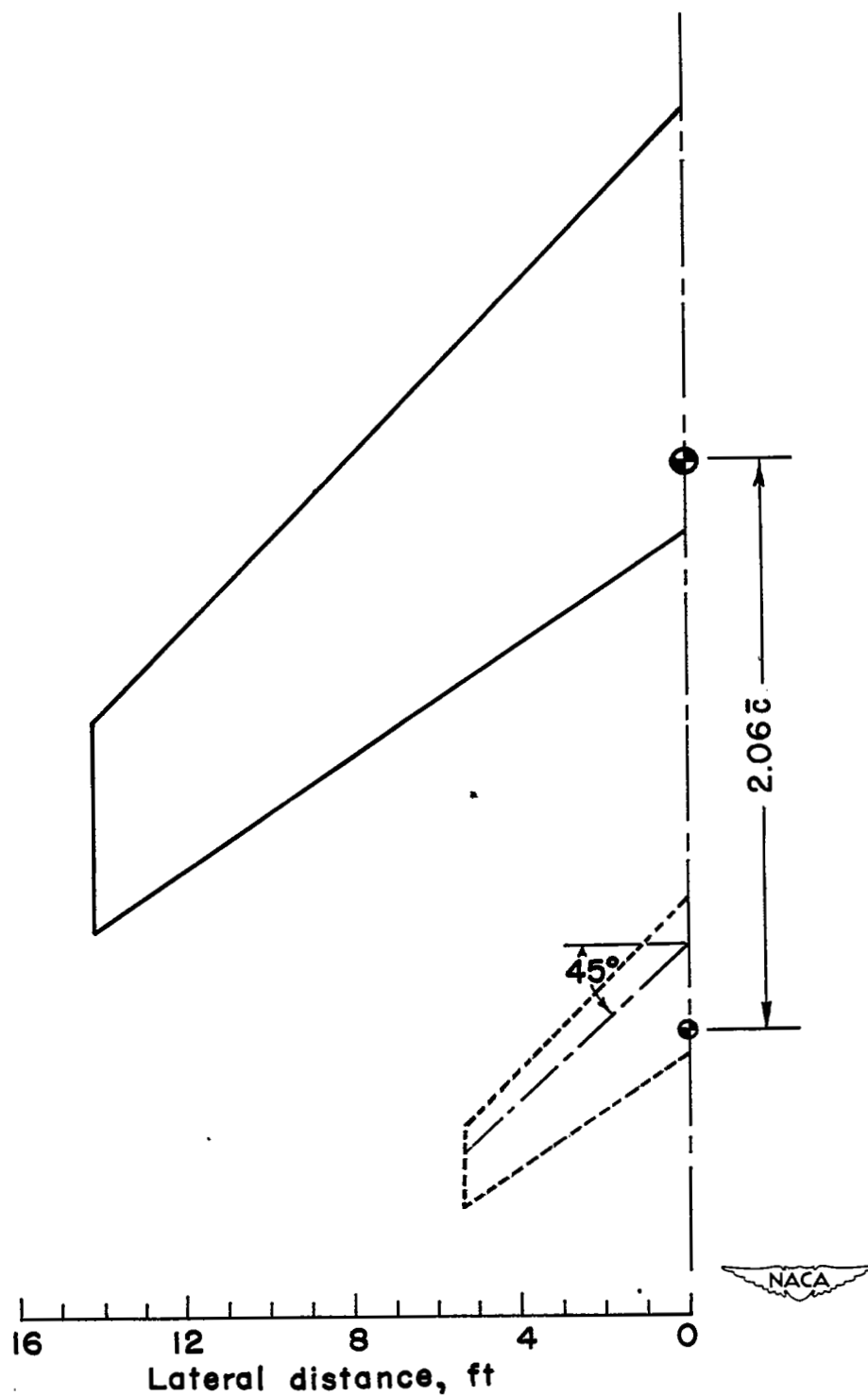
Figure 31.- Longitudinal location of the horizontal tail.
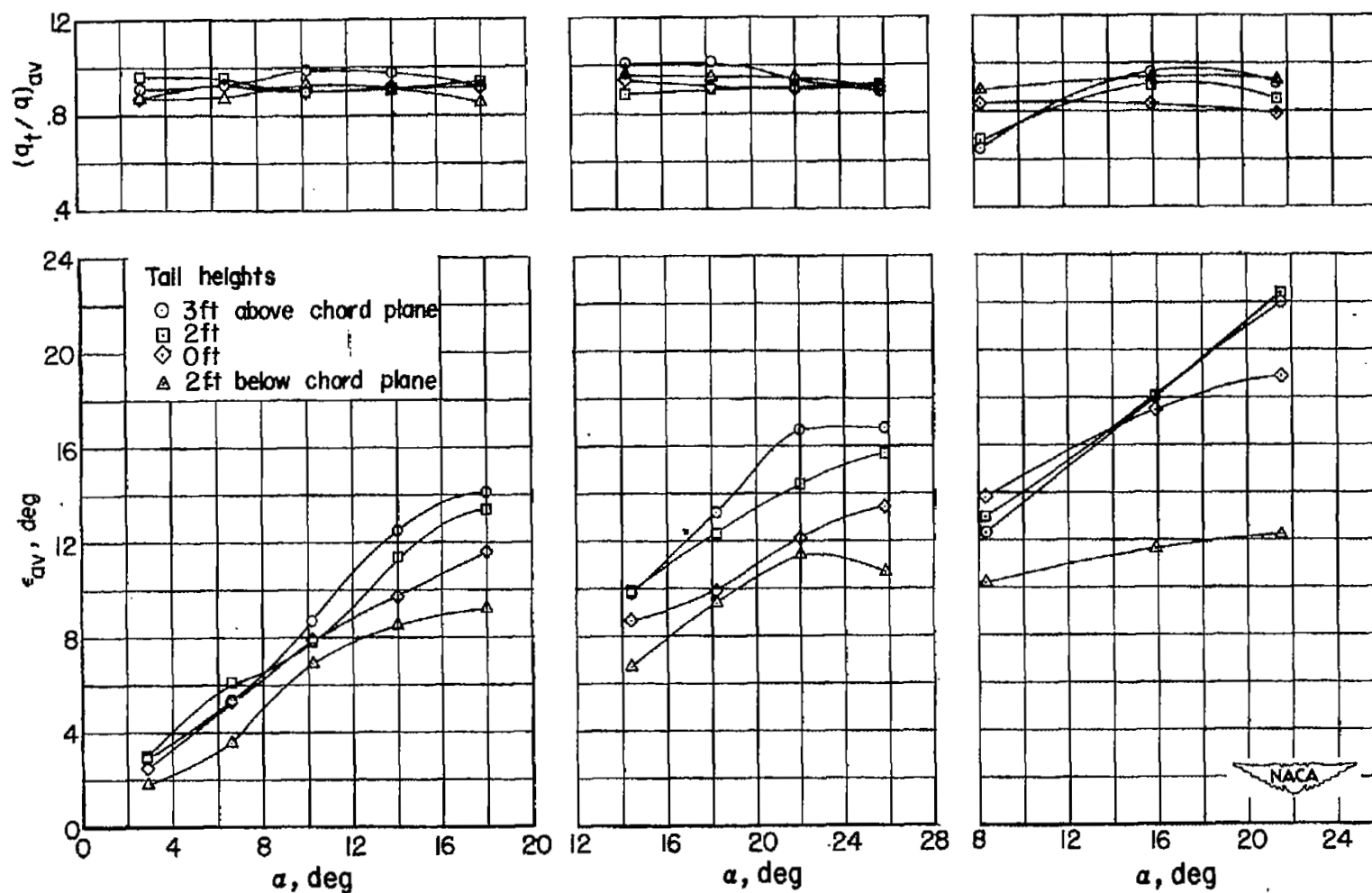
(a) Basic wing.

(b) Drooped-nose flaps deflected 40°.

(c) Drooped-nose and semispan plain flaps deflected 40°.

Figure 32.- Variation of average downwash angle and dynamic-pressure ratio with angle of attack.
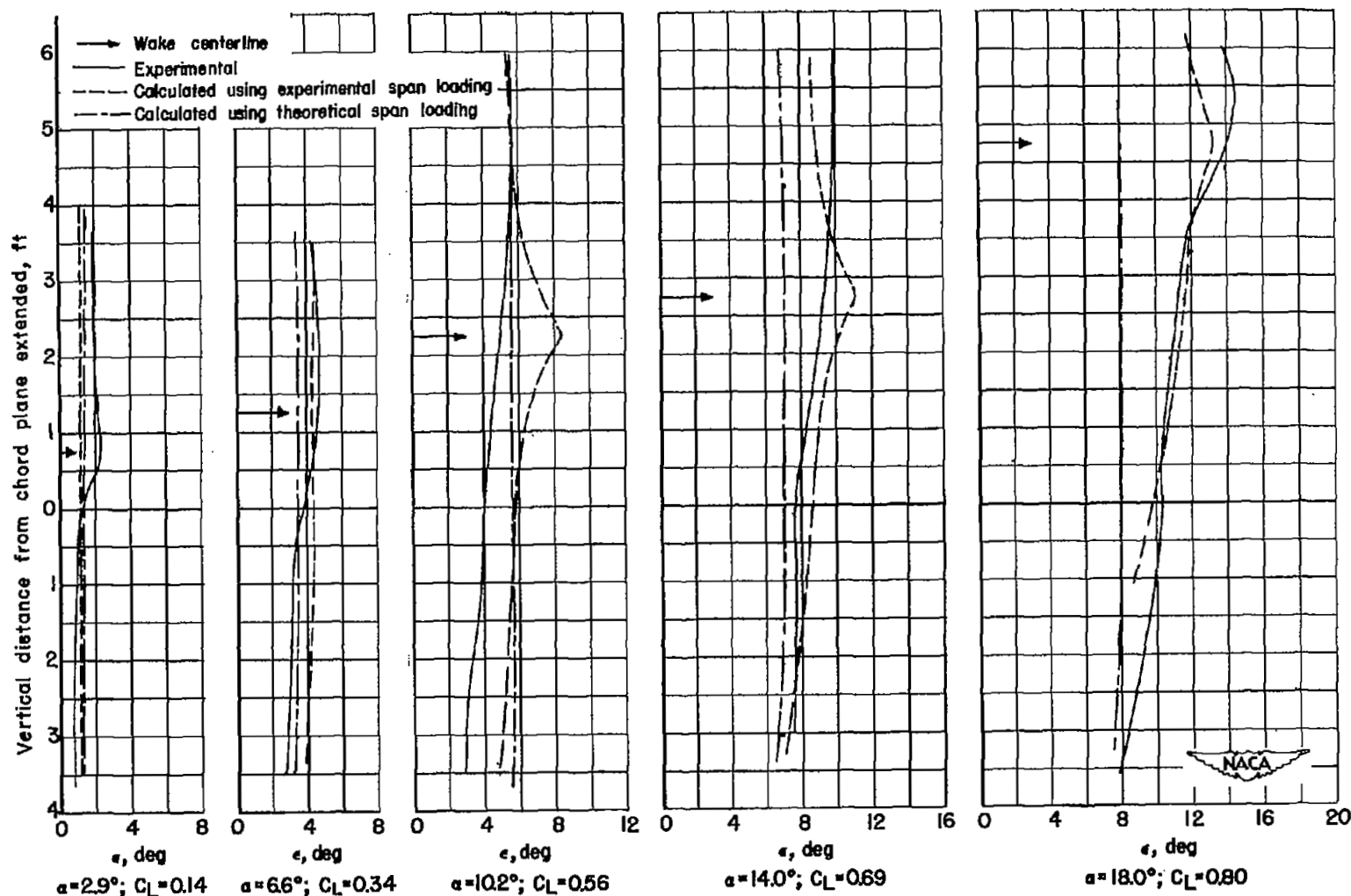
Figure 33.- Variation of experimental and calculated values of downwash
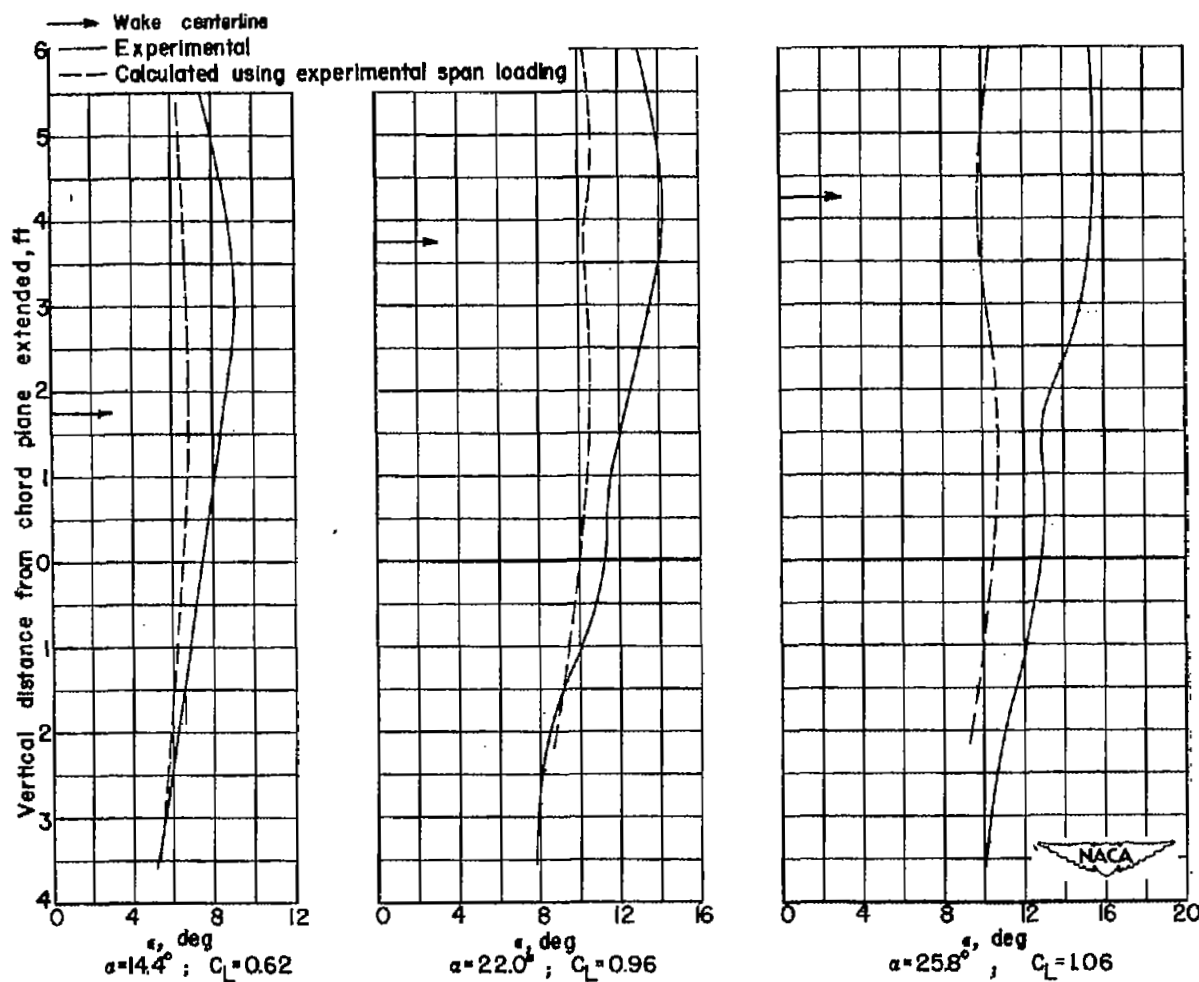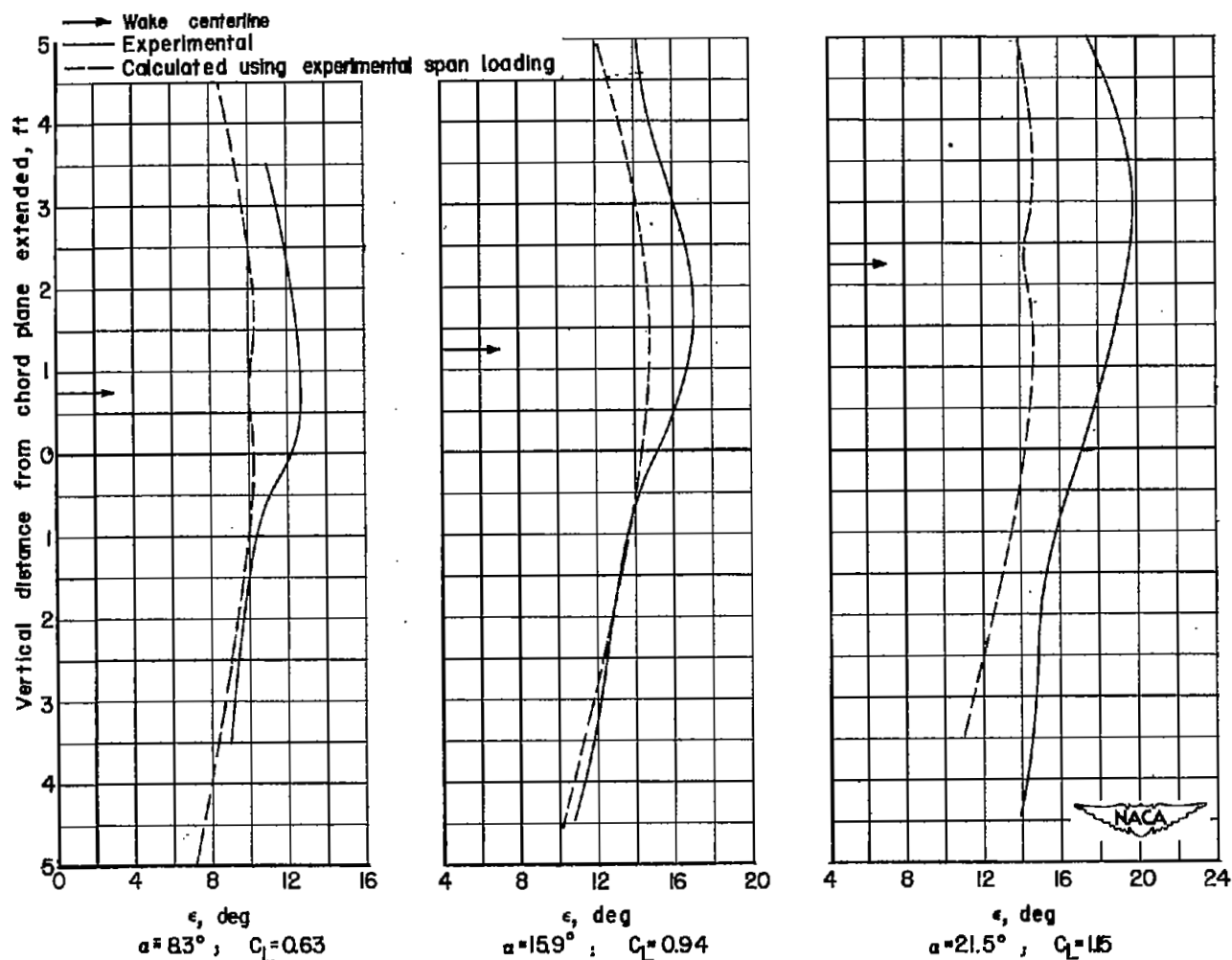with vertical distance at the plane of symmetry. Basic wing; longi-
tudinal location, 1.925$\bar{c}$.

Figure 34.- Variation of experimental and calculated values of downwash with vertical distance at plane of symmetry. Drooped-nose flap deflected 40°; longitudinal location, 1.925c̄.

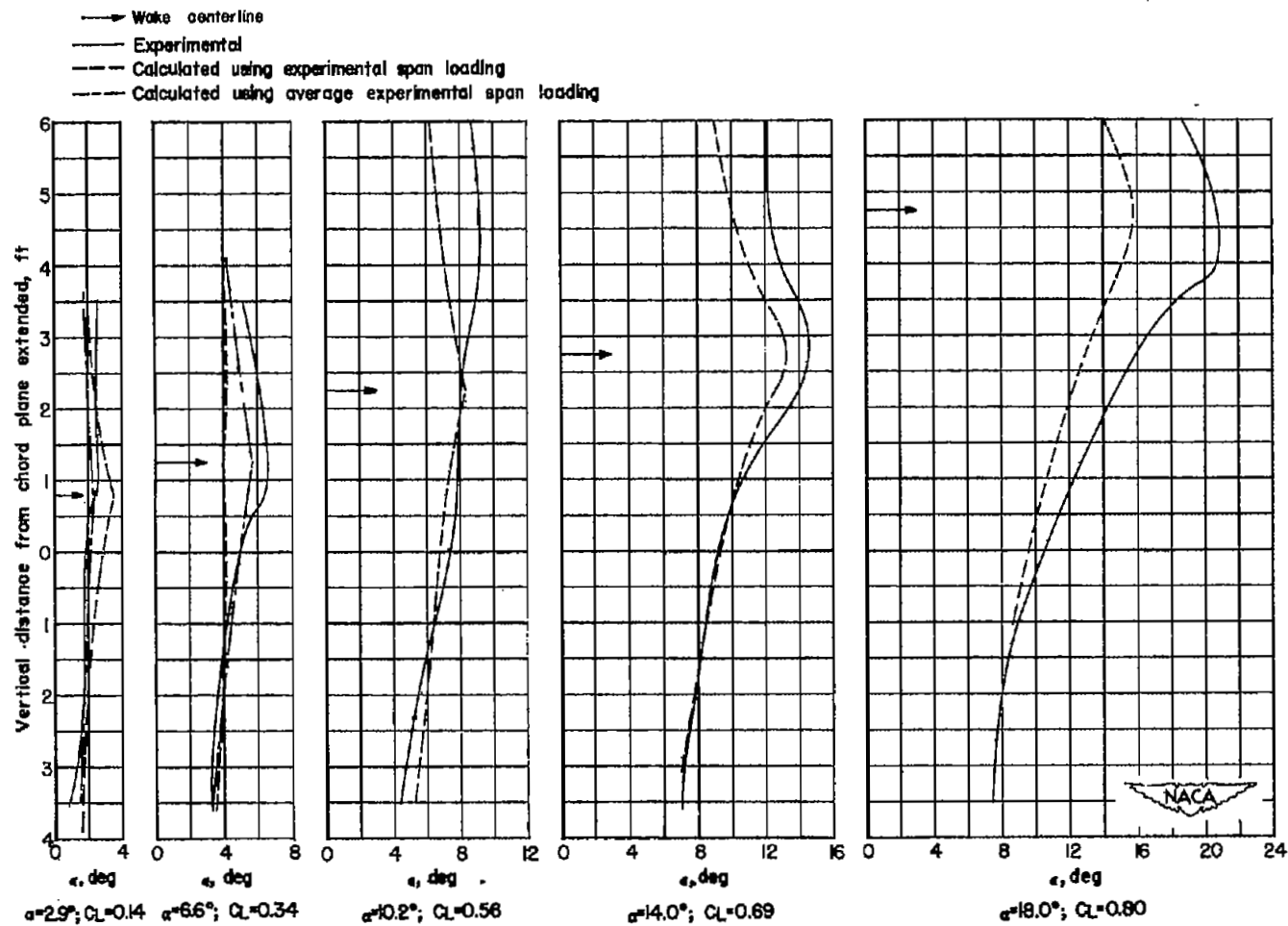Figure 35.- Variation of experimental and calculated values of
downwash with vertical distance at plane of symmetry. Drooped-
nose flaps and semispan plain flaps deflected 40°; longitudinal
location, 1.925$\bar{c}$.

Figure 36.- Variation of experimental and calculated values of downwash with vertical distance at $\frac{2y}{b} = 0.28$. Basic wing; longitudinal location, $1.925\bar{c}$.
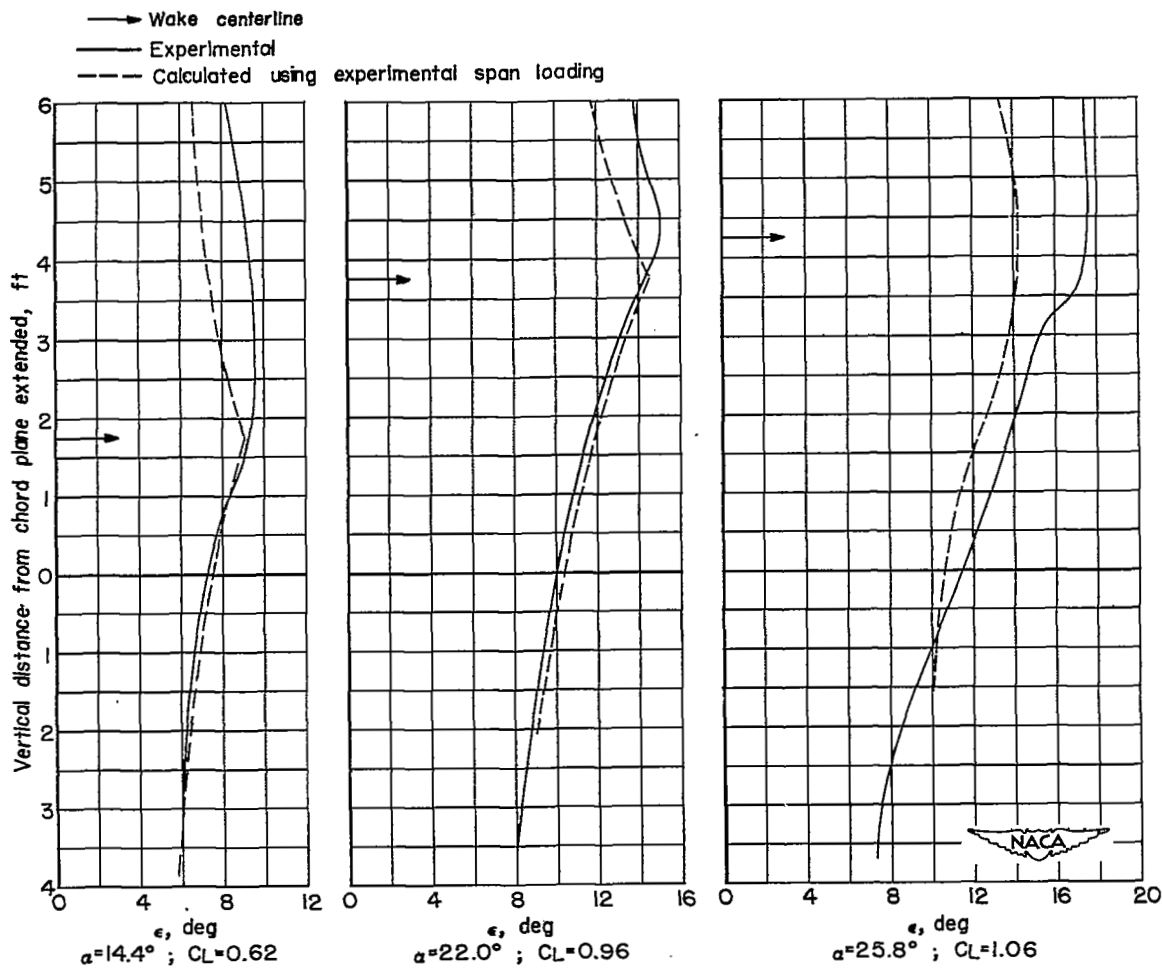
Figure 37.- Variation of experimental and calculated values of downwash with vertical distance at $\frac{2y}{b}$ = 0.28. Drooped-nose flap deflected 40°; longitudinal location, 1.925$\bar{c}$.
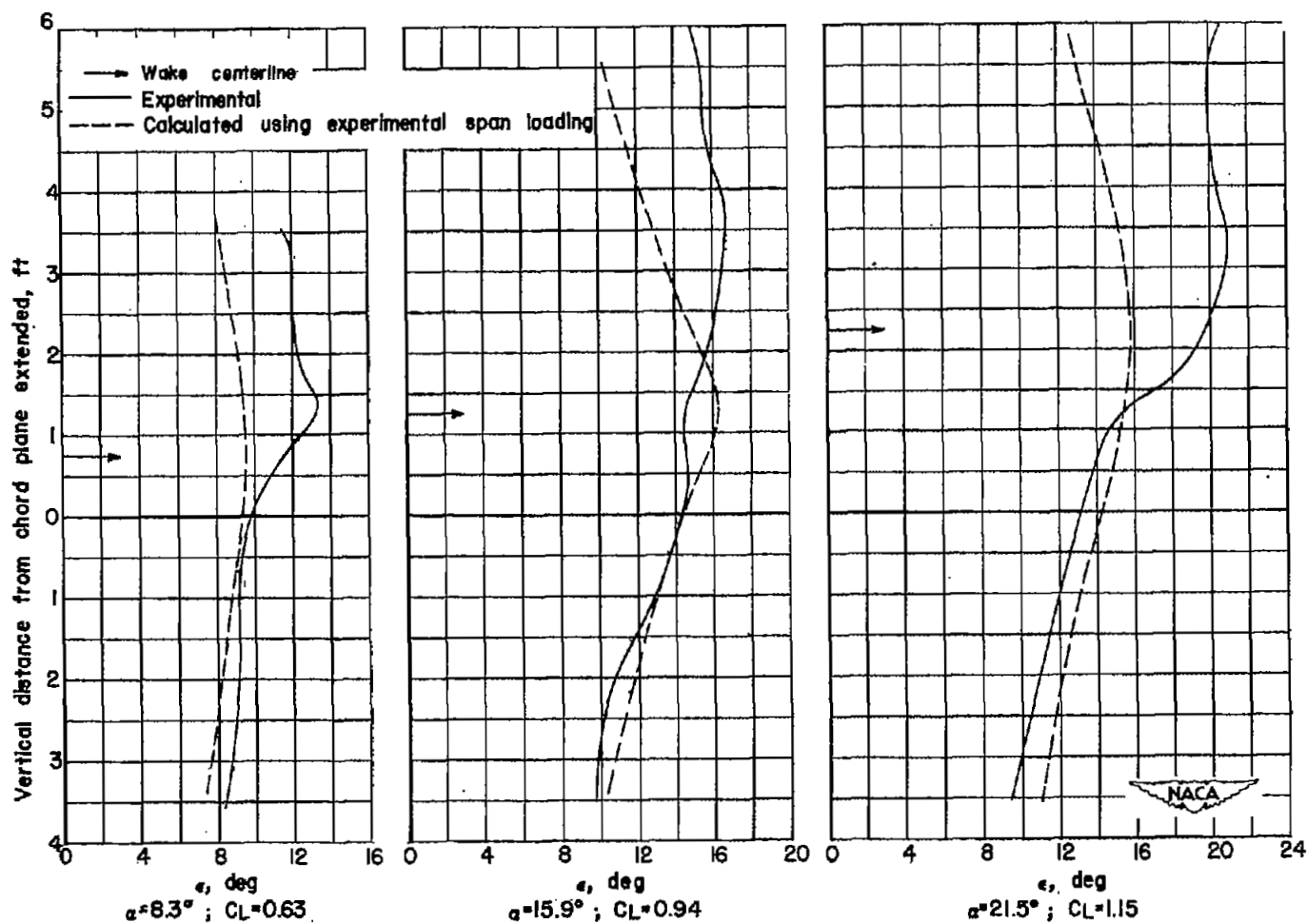
Figure 38.- Variation of experimental and calculated values of downwash with vertical distance at $\frac{2y}{b} = 0.28$. Drooped-nose flaps and semispan plain flaps deflected $40°$; longitudinal location, $1.925\bar{c}$.
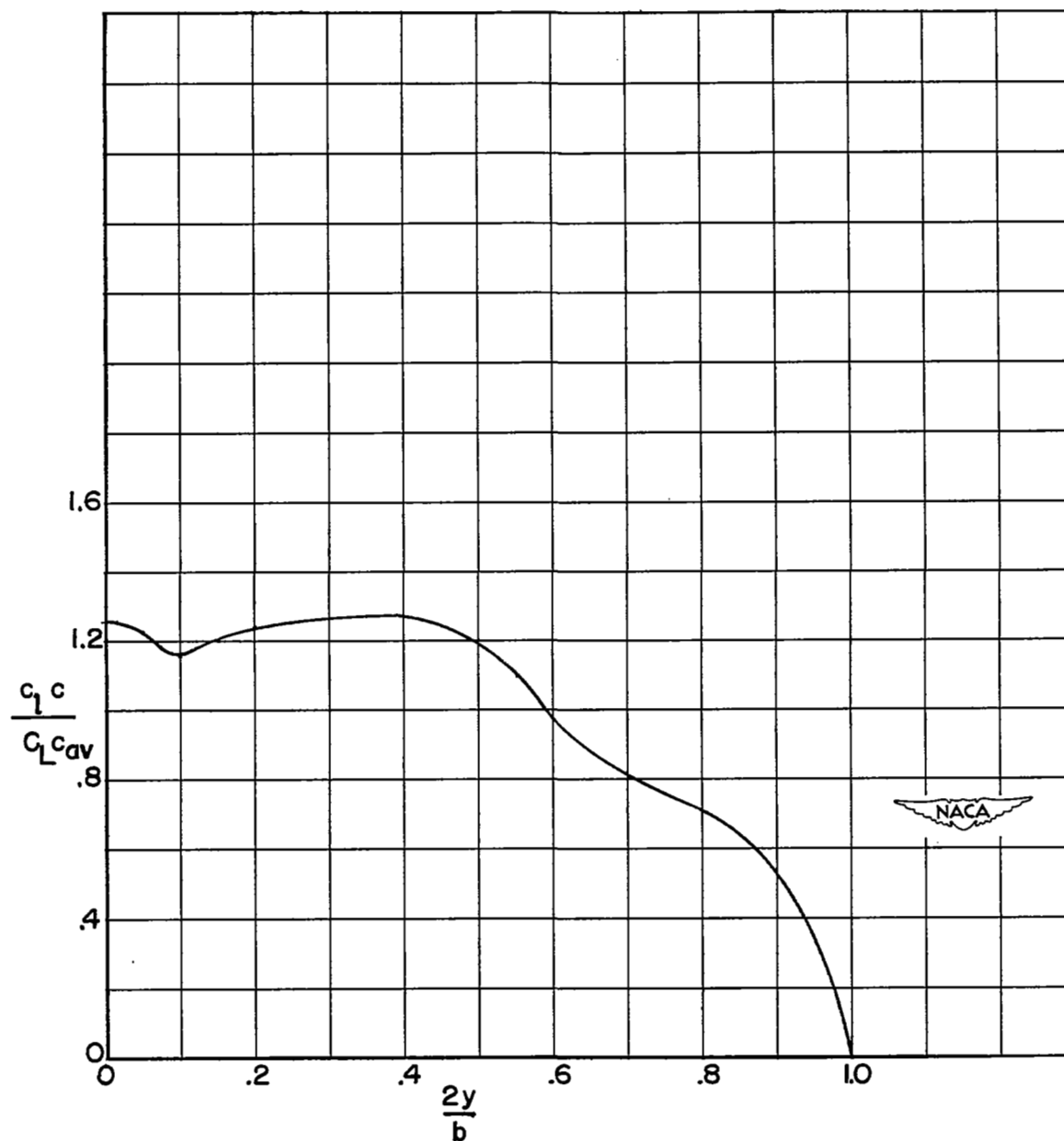
Figure 39.- Span load distribution obtained by averaging the loadings
    measured at low angles of attack for the basic wing configuration.